Journal of Hydrology

Geochemical and isotopic characterization of the shallow aquifers from the Mugello Basin (Tuscany, central Italy): implications for assessing a monitoring network in a seismically active area

--Manuscript Draft--

Manuscript Number:	HYDROL56982
Article Type:	Research paper
Keywords:	Mugello Basin, hydrogeochemistry, seismic tracers, earthquakes
Corresponding Author:	Lorenzo Chemeri University of Urbino Carlo Bo Department of Applied and Pure Sciences ITALY
First Author:	Lorenzo Chemeri
Order of Authors:	Lorenzo Chemeri
	Jacopo Cabassi
	Franco Tassi
	Francesco Capecchiacci
	Andrea L. Rizzo
	Stefano Caliro
	Orlando Vaselli
Abstract:	The Mugello Intermontane Basin (MIB) is located 30 km north of Florence (Tuscany, central Italy) and shows high seismicity with historical events characterized by Mw ≥ 6, e.g., on June 13, 1542 (Mw = 6.0) and June 29, 1919 (Mw = 6.4). Progresses in the identification of seismic tracers in geofluids has been made in the last decades, although reference values for a given area are necessary to assess hydrogeochemical anomalies prior to earthquakes. In this study, a detailed characterization of the chemical and isotopic composition of the natural waters discharging from MIB was performed. The aims were to (i) constrain the geochemical processes controlling the chemistry of waters and dissolved gases, (ii) assess the influence of deep-seated fluids in the shallow environment, and (iii) evaluate the suitability of geochemical parameters as reliable tracers for seismic activity. Two different types of waters were recognized, being characterized by: (A) calcium-bicarbonate (Ca-HCO3) composition, positive Eh values (150-200 mV), slightly alkaline pH (<8.3), and an N2-dominated dissolved gas phase; (B) sodium-bicarbonate waters (Na-HCO3,) composition, negative Eh (< -180 mV), pH>8.5, high contents in F, B and Li, and enrichments in dissolved CO2 and CH4. The chemistry of waters of group (A) is controlled by dissolution processes involving carbonate rocks, whilst the Na-HCO3waters likely result by prolonged water-silicate rock interactions and probably associated with longer circulation pathways. Argon (40Ar/36Ar) and carbon (δ13C in CO2 and CH4) isotopes indicate a predominant circulation within local aquifers by shallow fluids. Instead, helium (3He/4He) isotopes in dissolved gases highlighted a contribution up to 6% by mantle/magmatic fluids probably rising through deep faults. The results obtained suggest that trace elements and the isotopic signatures of dissolved CO2, CH4, and He may represent reliable seismic tracers for the MIB on the basis of which a monitoring network could be deployed.

1506
UNIVERSITÀ DEGLI STUDI DI URBINO CARLO BO
DISPEA
DIPARTIMENTO DI SCIENZE PURE E APPLICATE

Dear Editor,

We are pleased to submit to the *Journal of Hydrology* the research article titled: "***Geochemical and isotopic characterization of the shallow aquifers from the Mugello Basin (Tuscany, central Italy): implications for assessing a monitoring network in a seismically active area***" by Lorenzo Chemeri, Jacopo Cabassi, Franco Tassi, Francesco Capecchiacci, Andrea L. Rizzo, Stefano Caliro and Orlando Vaselli.

This paper presents and discusses the results obtained from a detailed geochemical and isotopic characterization of spring and well waters discharging in the Mugello Basin (Tuscany), one of the most seismically active areas in central Italy. The aims were to (i) constrain the main geochemical processes acting in the area, (ii) investigate the possible interplay between deep-originated fluids and shallow aquifers, and (iii) assess the possible use of geochemical parameters as tracers for seismic activity. To the best of our knowledge, this study represents the very first geochemical and isotopic investigation in the Mugello area and has a broad interest for the definition and the development of a water monitoring network aimed at identifying possible seismic tracers, one of the most discussed and studied aspect of geosciences. We consider this study to be useful in improving and expanding the knowledge on the possible relationships between fluid geochemistry and seismic events; consequently, we hope that this manuscript can be considered suitable for publication in the Journal of Hydrology.

All the authors have read the paper and it has not been published or submitted elsewhere. All the authors approved the content of this work. This study did not involve human or animal subjects.

Best regards,

Lorenzo Chemeri

On behalf of all the Authors

Dr. Lorenzo Chemeri
Via Ca' Le Suore, 2/4 - 61029 Urbino PU, Italy
Tel. +39 3200207985
Lorenzo.chemeri@campus.uniurb.it

Declaration of interests

☒The authors declare that they have no known competing financial interests or personal relationships that could have appeared to influence the work reported in this paper.

☐The authors declare the following financial interests/personal relationships which may be considered as potential competing interests:

Highlights (3 to 5 bullet points (maximum 85 characters including spaces per bullet point)

Highlights

(1) Mugello Basin (MIB) is one of the most seismically active areas in central Italy

(2) Ca-HCO_3 and Na-HCO_3 waters circulate in the MIB groundwater system

(3) The influence of deep-seated fluids in shallow aquifers is currently negligible

(4) Trace elements and dissolved gas isotopes are regarded as good seismic tracers

Abstract

The Mugello Intermontane Basin (MIB) is located 30 km north of Florence (Tuscany, central Italy) and shows high seismicity with historical events characterized by $M_w \geq 6$, e.g., on June 13, 1542 ($M_w = 6.0$) and June 29, 1919 ($M_w = 6.4$). Progresses in the identification of seismic tracers in geofluids has been made in the last decades, although reference values for a given area are necessary to assess hydrogeochemical anomalies prior to earthquakes. In this study, a detailed characterization of the chemical and isotopic composition of the natural waters discharging from MIB was performed. The aims were to (i) constrain the geochemical processes controlling the chemistry of waters and dissolved gases, (ii) assess the influence of deep-seated fluids in the shallow environment, and (iii) evaluate the suitability of geochemical parameters as reliable tracers for seismic activity. Two different types of waters were recognized, being characterized by: (A) calcium-bicarbonate (Ca-HCO_3) composition, positive Eh values (150-200 mV), slightly alkaline pH (<8.3), and an N_2-dominated dissolved gas phase; (B) sodium-bicarbonate waters (Na-HCO_3,) composition, negative Eh (< -180 mV), pH>8.5, high contents in F, B and Li, and enrichments in dissolved CO_2 and CH_4. The chemistry of waters of group (A) is controlled by dissolution processes involving carbonate rocks, whilst the Na-HCO_3 waters likely result by prolonged water-silicate rock interactions and probably associated with longer circulation pathways. Argon ($^{40}Ar/^{36}Ar$) and carbon ($\delta^{13}C$ in CO_2 and CH_4) isotopes indicate a predominant circulation within local aquifers by shallow fluids. Instead, helium ($^3He/^4He$) isotopes in dissolved gases highlighted a contribution up to 6% by mantle/magmatic fluids probably rising through deep faults. The results obtained suggest that trace elements and the isotopic signatures of dissolved CO_2, CH_4, and He may represent reliable seismic tracers for the MIB on the basis of which a monitoring network could be deployed.

Geochemical and isotopic characterization of the shallow aquifers from the Mugello Basin (Tuscany, central Italy): implications for assessing a monitoring network in a seismically active area

Chemeri Lorenzo[a,d], Cabassi Jacopo[b], Tassi Franco[a,b], Capecchiacci Francesco[a,b,f], Rizzo Andrea L.[c,e], Caliro Stefano[f], Vaselli Orlando[a,b]

(a) *Department of Earth Sciences, University of Florence, Via G. La Pira 4, 50121, Florence, Italy*

(b) *Institute of Geosciences and Earth Resources (IGG), National Research Council of Italy (CNR), Via G. La Pira 4, 50121, Florence, Italy*

(c) *Department of Earth and Environmental Sciences, University of Milano Bicocca, Piazza della Scienza 4, 20126, Milano, Italy*

(d) *Department of Pure and Applied Sciences, University of Urbino Carlo Bo, Via Ca' Le Suore 2/4, 61029, Urbino, Italy*

(e) *Istituto Nazionale di Geofisica e Vulcanologia (INGV), Sezione di Milano, Via Alfonso Corti 12, 20133, Milano, Italy*

(f) *Istituto Nazionale di Geofisica e Vulcanologia (INGV), Sezioni di Napoli, Osservatorio Vesuviano, Via Diocleziano, 328, 80124, Napoli, Italy*

Keywords: Mugello Basin, hydrogeochemistry, seismic tracers, earthquakes

Corresponding author: Lorenzo Chemeri (@l.chemeri@campus.uniurb.it)

Address: Department of Pure and Applied Sciences, University of Urbino, Via Ca' Le Suore 2/4, 61029, Urbino, Italy

Abstract

The Mugello Intermontane Basin (MIB) is located 30 km north of Florence (Tuscany, central Italy) and shows high seismicity with historical events characterized by $M_w \geq 6$, e.g., on June 13, 1542 ($M_w = 6.0$) and June 29, 1919 ($M_w = 6.4$). Progresses in the identification of seismic tracers in geofluids has been made in the last decades, although reference values for a given area are necessary to assess hydrogeochemical anomalies prior to earthquakes. In this study, a detailed characterization of the chemical and isotopic composition of the natural waters discharging from MIB was performed. The aims were to (i) constrain the geochemical processes controlling the chemistry of waters and dissolved gases, (ii) assess the influence of deep-seated fluids in the shallow environment, and (iii) evaluate the suitability of geochemical parameters as reliable tracers for seismic activity. Two different types of waters were recognized, being characterized by: (A) calcium-bicarbonate (Ca-HCO_3) composition, positive Eh values (150-200 mV), slightly alkaline pH (<8.3), and an N_2-dominated dissolved gas phase; (B) sodium-bicarbonate waters (Na-HCO_3,) composition, negative Eh (< -180 mV), pH>8.5, high contents in F, B and Li, and enrichments in dissolved CO_2 and CH_4. The chemistry of waters of group (A) is controlled by dissolution processes involving carbonate rocks, whilst the Na-HCO_3 waters likely result by prolonged water-silicate rock interactions and probably associated with longer circulation pathways. Argon ($^{40}Ar/^{36}Ar$) and carbon ($\delta^{13}C$ in CO_2 and CH_4) isotopes indicate a predominant circulation within local aquifers by shallow fluids. Instead, helium ($^3He/^4He$) isotopes in dissolved gases highlighted a contribution up to 6% by mantle/magmatic fluids probably rising through deep faults. The results obtained suggest that trace elements and the isotopic signatures of dissolved CO_2, CH_4, and He may represent reliable seismic tracers for the MIB on the basis of which a monitoring network could be deployed.

1. Introduction

Over the last decades, several studies evidenced that prior to intermediate and large earthquakes geochemical precursory phenomena, consisting of changes in the chemistry of underground circulating fluids, have been observed (Cicerone et al., 2009 and reference therein; Martinelli, 2020). These anomalies may occur from either weeks to months before any seismic event or during the event itself, suggesting that earthquakes and physical processes (i.e., faulting and micro-fracturing) can affect groundwater geochemistry and isotopes, springs flow rates and gas emission discharges (Wang and Manga, 2021 and reference therein). The main physical processes responsible for chemical variations of springs are represented by: (i) an increase in water-rock interaction due to the formation of active (fresh) rock surfaces (e.g., Claesson et al., 2004; Skelton et al., 2019) and (ii) water mixing between two or more physically-separated aquifers due to aquifer breaching and/or changes in the hydraulic head (e.g., Thomas, 1988; Reddy et al., 2017). On the other hand, hydrologic changes are generally related to permeability increase (or decrease) or unclogging of the flow paths, these variations being macroscopic and therefore easier to be detected. According to Martinelli (2000, 2020), the very first observations related to evident changes in fluid discharges before the occurrence of a seismic event dated back

to the Ancient Greeks. Such physical variations are generally transitory and, consequently, difficult to identify, being site-specific and exclusively related to a given area as a function of geological and structural features.

As a consequence, several fluid geochemistry-based pilot studies were launched in different geological and geodynamic environments worldwide characterized by intense seismic activity (e.g., Claesson et al., 2004; Skelton et al., 2014; Hosono et al., 2019). On the basis of periodical and/or continuous geochemical multi-parametric monitoring of springs and wells, promising results were achieved (e.g., Franchini et al., 2021; Gori and Barberio, 2022). For example, increase in Cr, As, V and other metals were detected prior to the 2016 Amatrice-Norcia seismic sequence in central Italy (e.g., Barberio et al., 2017), which caused the death of 303 persons. In Northern Iceland, significant changes in the $\delta^{18}O$- and $\delta^{2}H$-H_2O values were detected during and after a 5.8 M_w earthquake (Claesson et al., 2004). However, it is not possible to generalize because the geochemical context of each system behaves differently.

Strong increments in Rn soil emissions and/or Rn groundwater concentrations were repeatedly observed worldwide (e.g., Cicerone et al., 2009), whereas changes in CH_4 diffuse emissions from soils coupled with an increase in its $^{13}C/^{12}C$ ratio were reported to occur in the Emilia Region (Central Italy), in correspondence of the seismic sequence that affected this region in 2012 (Sciarra et al., 2017). The 1996-1997 Umbria-Marche seismic swarm was also marked by significant anomalies in dissolved mantle-derived helium (Italiano et al., 2001).

Thermal, cold and mineral springs and deep wells are commonly the preferred sites to be monitored since they are generally related to long-term fluid circulation pathways and limitedly affected by seasonal changes and anthropogenic activities (i.e., well-pumping or water contamination). Nevertheless, shallow waters are also monitored since they are generally always available and accessible (Thomas, 1988).

Italy is one of the most seismically active countries in the world and the fourth country with the highest economic loss (a total of $66 billion) due to natural disasters, with almost half of them caused by earthquakes (CRED, 2018). According to the latest DISS (*Database of Individual Seismogenic Sources*) version, one of the most dangerous areas in Italy for seismic hazard is the 1.130 km^2 wide Mugello Intermontane Basin (hereafter, MIB), located in the Northern Apennines, ca. 30 km north of Florence (Tuscany, central Italy).

MIB is characterized by the presence of individual and composite seismogenic sources able to generate earthquakes larger than M_w 5.5 (Sani et al., 2009; DISS Working Group, 2021; Saccorotti et al., 2022). Several seismic events have recently occurred, some of them being characterized by a magnitude $\geq$ 6.0 M_w, e.g., on June 13, 1542 (6.0 M_w) and June 19, 1919 (6.4 M_w), the latter causing more than one hundred fatalities and severe damages throughout the basin area (Rovida et al., 2020, 2021). In recent years (2008-2019), MIB experienced four seismic sequences during which magnitudes ranging from 4.2 up to 4.5 were recorded (Saccorotti et al., 2022). Improving the assessment of seismic hazards is extremely important given the demographic, cultural, and economic relevance of the study area. In fact, more than 60,000 people live in MIB, which is located close to highly urbanized areas such as the Metropolitan area of Florence. Additionally, two major infrastructures cross MIB: the A1 Motorway (*Autostrada del Sole*) and the high-speed railway (TAV),

both neuralgic for national transportation since they are the main communication lines connecting the northern and central-southern sectors of Italy.

This paper is aimed at characterizing the geochemical and isotopic composition of spring and well waters and dissolved gases in order to (i) define the hydrogeological pathways, (ii) investigate the interplay between deep-originated fluids and shallow aquifers, and (iii) evaluate which geochemical parameters can be regarded as possible and suitable seismic tracers and envisage a monitoring geochemical and isotopic network that is presently missing.

2. Geodynamic and geological setting

MIB is a WNW-ESE-trending asymmetric graben (25x15 km wide) developed on the western flank of the Northern Apennines belt (Martini and Sagri, 1993: Benvenuti 1995, 1997, 2003; Benvenuti and Papini, 1997). It is drained by the Sieve River, one of the major tributaries of the Arno River. MIB, consisting of two sub-basins (Barberino – BSB and Borgo San Lorenzo BSLSB, Benvenuti, 1997), is characterized by a complex tectonic setting, being bordered by two tectonic alignments, i.e., the Livorno-Sillaro tectonic lineament to the W and the Piombino-Faenza line to the E. The geological evolution of MIB is related to an extensional phase that started in the latest Upper Pliocene (Sestini, 1970), while during the Lower Pleistocene, it predominantly developed under a tectonic compressional regime, alternating with, or suppressing, crustal extension (Boccaletti et al., 1999; Sani et al., 2009). The final evolutionary and still active stage of MIB has been operating since the Middle Pleistocene with an extensional normal faulting tectonics, which locally superimposed onto the former compressive structures (Sani et al., 2009). The main macrostructural elements are low-angle thrusts, being often obliterated or dislocated by subsequent high-angle tectonics, and involve both transverse (NE-SW) and longitudinal (NW-SE) high-angle faults (Boccaletti et al., 1999; Sani et al., 2009). The recent seismicity in the area is likely related to three major fault systems active since the Early Pleistocene (Delle Donne, 2005; Fig. 1), namely (i) the Ronta fault system in the NE margin, (ii) the Sieve fault system at the S margin, and (iii) the Vicchio fault system, delimitating MIB at SE (Sani et al., 2009). The Ronta Fault system consists of ca. 20-25 km long parallel steeply dipping normal faults, affecting the pre-basin substratum (primarily made of Miocene sandstones) at the NE basin margin (Saccorotti et. al, 2022) and being superimposed onto the NE-verging contractional structures (Sani et al., 2009). The Ronta fault system is considered responsible of the biggest earthquakes, including the one that hit the area in 1919 (Bonini et al., 2016), although the concurrent activation of transverse faults may not be excluded (Delle Donne, 2005; Sani et al., 2009).

The MIB substratum consists of tectono-sedimentary units piled up in a NE-verging and NW-SE trending thrust sheet system developed during the Tertiary (Vai, 2001) (Fig. 1). The NE margin of MIB includes Paleocene-Eocene calcareous turbidites encasing chaotic claystones with limestones and serpentinite blocks (Ligurid units), tectonically overlying Early-Middle Miocene turbiditic sandstones and siltstones (Cervarola-Falterona and Castel Guerrino Unit). On the southern and southwestern margins of the basin, the Tuscan units

(Galiga, Acquerino, and Cervarola-Falterona units) are capped through a thrust fault by Oligocene-early Miocene calcareous and terrigenous coarse-grained turbiditic deposits (Sub-Ligurid units) (Benvenuti, 1997, 2003). These tectonic units represent the substratum on which the fluvio-lacustrine (Mugello synthem) and alluvial (Sieve River synthem) deposits of MIB lie in unconformity (Fig. 1) (Benvenuti 1997, 2003; Bortolotti et al., 2010). To the best of our knowledge, the hydrogeological features of MIB are extremely scarce (e.g., Rodolfi, 2006). The springs occurring in the MIB can be grouped into the following categories: (i) waters discharging from either slope deposits or limited fractured systems, associated with shallow circulation patterns. Hence, their activity is extremely influenced by seasonality and rainfall events, (ii) springs with wider supply basins, characterized by constant flow rates likely related to deeper circulation pathways influenced by the main fractured systems, slightly influenced by seasonality, which generally supply the aqueduct network, (iii) springs that formed following permeability contrasts between different lithologies. They mostly occur at stratigraphic or tectonic limits between marly-sandstone and marly-calcareous lithologies and geological formations dominated by the pelitic component, and eventually, (d) sulfur springs, with a different chemical character, showing limited, though perennial, flows (Rodolfi et al., 2006).

3. Materials and Methods

Forty-one waters were collected during three surveys between July and September 2020 (Tab.1), as follows (Fig. 2): 31 cold springs, 2 mud volcano-related waters, 2 wells (one of which at ca. 80 m deep), and 6 springs, characterized by a strong odor of rotten eggs and the presence of colloidal sulfur at the emergence, that given their peculiar features, are referred as sulfur springs (Figs. 2A, B, C). In most cases, the cold springs are characterized by low flow rates, generally < 2 L/s (Figs. 2D, E, F).

The main physicochemical parameters, i.e., temperature (°C), pH, electrical conductivity (EC), and redox potential (ORP), were determined *in situ* using a *Crison* 2000 multiparametric probe. At each sampling point, different aliquots were collected, as follows: (i) unfiltered aliquot in 125 mL polyethylene (PE) bottle for the analysis of the main anions and NH_4^+; (ii) filtered (0.45 μm) and acidified (with 1% Suprapur HCl) aliquot in 50 mL PE bottle for the analysis of the main cations; (iii) filtered (0.45 μm) and acidified (with 1% Suprapur HNO_3) aliquot in 50 mL PE bottle for trace elements (i.e., SiO_2, Li, B, Fe, Mn, Sr, As); (iv) unfiltered aliquot in 15 mL plastic tube for the analysis of the water isotopes; (v) unfiltered aliquot in pre-evacuated 250 mL glass flasks equipped with Thorion® valves for the analysis of dissolved gases following the method proposed by Capasso and Inguaggiato (1998) and Tassi et al. (2009).

Carbonate alkalinity was analyzed by acidimetric titration (AT) using an automatic burette filled with 0.01 M HCl and methyl-orange as an indicator. The main cations (Ca^{2+}, Mg^{2+}, Na^+, K^+) and anions (Cl^-, SO_4^{2-}, Br^-, F^-, NO_3^-) were determined by ion chromatography (IC), using Metrohm 861 Compact IC and Metrohm 761 Advanced Compact IC chromatographs, respectively. Ammonium (NH_4^+) was analyzed by molecular spectrophotometry (MSP, Nessler Method) using a HACH DR2100 instrument. The analytical errors for AT,

IC, and MSP were below 5%. Trace elements were measured by ICP-MS (inductively coupled plasma mass spectrometry) using an Agilent 7800 mass spectrometer, and the analytical error was below 10%.

The gas compounds stored in the headspace of the sampling flasks were analyzed by gas chromatography (GC), using different instruments, as follows: i) CO_2, N_2, ($Ar+O_2$) and He with a Shimadzu 15A equipped with a 5 m long stainless-steel column with Porapak 80/100 mesh and a TCD; ii) Ar and O_2 via a Thermo Focus equipped with a 30 m long capillary molecular sieve column and a TCD; iii) CH_4 through a Shimadzu 14A equipped with a FID and a 10 m long stainless-steel-column packed with Chromosorb PAW 80/100 mesh coated with 23% SP 1700 (Vaselli et al., 2006). The concentrations of dissolved gases (in μmol/L) were given by the sum of $n_{i;g}$, i.e. the moles of the *i* gas in the sampling flasks headspace measured by GC, and $n_{i;l}$, i.e. the moles of the *i* gas that remained in the water collected in the sampling flasks. The $n_{i;l}$ values were recalculated from the $n_{i;g}$, by means of Henry's law constants (Wilhelm et al., 1977), assuming that the separated gas phase was in equilibrium with the liquid phase (Vaselli et al., 2006).

The isotopic analysis of oxygen ($^{18}O/^{16}O$, expressed as $\delta^{18}O‰$ vs. V-SMOW) and hydrogen ($^{2}H/^{1}H$, expressed as $\delta^{2}H‰$ vs. V-SMOW) of the water molecule was performed with a near-infrared laser analyzer (Picarro L2130-i) using wavelength-scanned cavity ring-down spectroscopy technique (WS-CRDS, analytical errors: $\delta^{2}H$ ±0.5‰, $\delta^{18}O$ ±0.08‰ vs. V-SMOW). The isotopic analysis of carbon ($^{13}C/^{12}C$) in both carbon dioxide (CO_2) and methane (CH_4), expressed as $\delta^{13}C\text{-}CO_2$ and $\delta^{13}C\text{-}CH_4$ ‰ vs. V-PDB, respectively, was carried out through WS-CRDS using a Picarro G2201-i. The analytical errors for WS-CRDS were ±0.16‰ and ±1.15‰ vs. V-PDB for $\delta^{13}C\text{-}CO_2$ and $\delta^{13}C\text{-}CH_4$, respectively.

The isotopic composition of helium ($^{3}He/^{4}He$) in dissolved gases was determined using a Helix SFT-GVI mass spectrometer. The sample preparation followed the method proposed by Inguaggiato and Rizzo (2004). The data are expressed as R/Ra values, where R is the $^{3}He/^{4}He$ ratio measured in the sample and R_a is the $^{3}He/^{4}He$ ratio in the air (1.39×10^{-6}; Mamyrin and Tolstikhin, 1984). The helium isotopic ratio was corrected for air contamination (R_c/R_a) using the $^{4}He/^{20}Ne$ ratio determined for each sample (Poreda and Craig, 1989), according to the following formula:

$$R_c/R_a = [(R_M/R_a)(He/Ne)_M - (He/Ne)_A] / [(He/Ne)_M - (He/Ne)_A]$$

where R_c stands for air-corrected $^{3}He/^{4}He$ ratio, and subscripts M and A represent measured and atmospheric theoretical values, respectively.

The ^{20}Ne content was measured through a Helix MC-Plus Thermo, which is able to resolve the interference on mass 20 due to $^{40}Ar^{2+}$. The Ar-isotope composition was determined using a Helix MC-GVI mass spectrometer. More details on the analytic procedure are reported in Rizzo et al. (2015a and references therein). The analytical error on the $^{3}He/^{4}He$ ratio was generally below 2% while that of $^{40}Ar/^{36}Ar$ was <0.16%.

All chemical and isotopic analyses of waters and dissolved gases were carried out at the Laboratory of Fluid Geochemistry of the Department of Earth Sciences (University of Florence, Italy), except those of (a) $\delta^{18}O\text{-}H_2O$ and $\delta^{2}H\text{-}H_2O$, performed at the Laboratory of Fluids Geochemistry INGV-OV (Istituto Nazionale di

Geofisica e Vulcanologia – "Osservatorio Vesuviano", Naples, Italy); (b) the helium and argon isotopic ratios, measured at the INGV Noble Gas Laboratories of Palermo (Italy); and (c) trace elements concentrations at the laboratories of Gruppo C.S.A. Ltd. (Rimini, Italy).

4. Results

4.1 Water chemical and isotopic composition

According to Fig. 3 and the data reported in Tab. 2, most wasters (i.e., cold springs, mud volcanos and one well) showed a calcium-bicarbonate composition (Ca-HCO_3, hereafter *Group A*), whereas the waters collected from sulfur springs (with the exception of TAR sample) and that from the 80 m-deep well (PI-P) had a sodium-bicarbonate composition (Na-HCO_3, hereafter *Group B*). The TDS values of *Group A* ranged from 158 to 787 mg/L, whereas those of *Group B* were from 570 to 895 mg/L. Noteworthy, waters from *Group A* showed a slightly alkaline pH (generally below 8.3) and positive ORP values (between 150-200 mV), whereas waters from *Group B* presented an alkaline pH (above 8.5) and negative Eh values (below -180 meV). Carbonate alkalinity showed a large variability from 66 to 512 mg/L. Similarly, SO_4 varied from 5.7 to 98 mg/L, Cl ranged from 7.4 to 36 mg/L, and NO_3 was from 0.01 to 58 mg/L.

As far as cations are concerned, the Ca content was varying from 7 to 155 mg/L, being the most abundant component in all the samples belonging to *Group A*. The concentration of Na was below 20 mg/L for *Group A*, while it was the main cation in the samples belonging to *Group B* and ranging from 140 to 230 mg/L. The content of Mg was from 2.1 to 33 mg/L, and that of K spanned from <1 up to 4.4 mg/L. The SiO_2 content was comprised between 6.7 and 22 mg/L.

The concentrations of minor (e.g., F, Br) and trace elements (Tab. 3) were generally below the limit of detection (b.d.l.). Anomalous values of F, B, and Li (up to 4.6 mg/L, 1050 μg/L and 117 μg/L, respectively) were detected for those samples belonging to *Group B*, which also showed relatively low Sr contents (generally below 300 μg/L). In *Group A* waters, F was generally <1 mg/L, B <100 μg/L and Li was detected in concentrations ten times lower than those of *Group B*. Iron, Mn, and As were generally below the detection limit, i.e., below 5, 1, and 0.1 μg/L, respectively. The highest contents in Fe and Mn were related to CS-S (801 μg/L) and TAR (209 μg/L), respectively. As reached the peak value at PI-P (5.5 μg/L).

The isotopic ratios of hydrogen (δ^2H) and oxygen ($\delta^{18}O$) are reported in Tab. 2. The $\delta^{18}O$ values were ranging from -8.29 to -6.23 ‰ V-SMOW, while those of δ^2H ranged from -56.6 to -40.7 ‰ V-SMOW.

4.2 Chemical and isotopic ($\delta^{13}C$-CO_2, $\delta^{13}C$-CH_4, $^3He/^4He$, $^{40}Ar/^{36}Ar$) composition of dissolved gases

The chemical and isotopic composition of dissolved gases is reported in Table 4. Molecular nitrogen was the main gas component (up to 821 μmol/L) in both *Group A* and *Group B*, apart from samples BAG and PAN-S where CH_4 was dominating. Contents of CO_2 and CH_4 were strongly dependent on the water type, as a matter

of fact, CO_2 concentrations in the *Group A* waters were generally one order of magnitude lower than those detected for *Group B*. Methane showed contents below 0.05 μmol/L (except TAR) in all samples from the *Group A*, while the *Group B* waters (except SAG) were characterized by CH_4 contents ranging from 57 to 615 μmol/L. Molecular oxygen was varying from 0.21 to 333 μmol/L, the lower contents being detected for *Group B*. The $\delta^{13}C\text{-}CO_2$ values ranged from -30 to -14 ‰ V-PDB, with no clear distinction between the two groups of waters. On the contrary, the $\delta^{13}C\text{-}CH_4$ data were characterized by a large variability, i.e., from -85 to -7.5 ‰ V-PDB, the less negative values pertaining to the *Group A* waters.

The He isotopic ratio not corrected for air contamination (expressed as R/R_a) ranged from 0.29 to 1.04 R_a, and $^4He/^{20}Ne$ varying between 0.33 and 1.99 (Fig. 4). Samples with the highest $^4He/^{20}Ne$ values (>1) showed the lowest R/R_a values (as low as 0.3 R_a) and the minimum bias between the R/R_a and the R_c/R_a values (0.13-0.28). No significant differences in terms of $^3He/^4He$ were observed between *Group A* and *Group B*. The $^{40}Ar/^{36}Ar$ isotopic ratios were clustering around the theoretical value of atmosphere-derived fluids (Air=298.6; Lee et al., 2006), being comprised between 294 and 302.

5. Discussion

5.1 Water geochemistry

As far as the isotopic composition of water is concerned (Fig. 5A), the samples are distributed following approximately the Central Italy Meteoric Water Line (CIMWL; Longinelli and Selmo, 2003), with some samples slightly shifted toward to the Mediterranean Meteoric Water Line (MMWL: Gat and Carmi, 1970), suggesting a clear meteoric-origin for these waters and excluding water-rock interaction processes at relatively high temperatures or the involvement of fossil or formation waters (e.g., Capaccioni et al., 2003).

In order to assess a possible influence due to both latitude and continental effect and identify the possible areas of recharge (e.g., Nisi et al., 2014), the $\delta^{18}O$ and δ^2H values were plotted vs. the altitude of the sampling sites (Fig. 5B-C), and that of oxygen was compared with three gradients available in the literature (Longinelli and Selmo, 2003; Minissale and Vaselli, 2011; Giustini et al., 2016). The oxygen and hydrogen isotopic gradient for these waters were computed using a *best-fit function* and they were 0.24 $\delta^{18}O$/100 m and nearly 1.00 δ^2H/100 m (Vespasiano et al., 2015; Natali et al., 2022). Following the sample distribution in Fig. 5B and 5C, it is possible to assume that the recharge area for the shallow groundwater system on the eastern flank of MIB is likely represented by the altitudes surrounding the FdA sample (also showing the lowest TDS value) and located ca. 200 m above the sampling points.

Waters from *Group A* show the typical chemical composition pertaining to surface and shallow aquifers (e.g., Martinelli et al., 1998; Minissale et al., 2000; Barth et al., 2003; Jeelani et al., 2011), and positive Eh values that indicate oxidizing conditions. Therefore, the geochemistry of *Group A* waters is mainly controlled by the dissolution of calcite and subordinately dolomite, as confirmed by the sample distribution in Fig. 6A, with

minor contributions deriving from both the congruent dissolution of anhydrite/gypsum (Fig. 6B) and the incongruent dissolution of silicate minerals. Moreover, an input deriving from anthropogenic activities (i.e., agriculture) cannot be excluded for those samples showing NO_3 concentration >10 mg/L, e.g., MdV, PI-S (e.g., Torres-Martínez et al., 2020, 2021). Contrarily, waters from *Group B* showed a sodium-bicarbonate composition (Na-HCO_3) with strong enrichment in both Na, not compensated by Cl (Fig. 7), and in carbonate species (HCO_3 and CO_3), not compensated by either Ca or Mg, which are strongly depleted in these samples with respect to the stoichiometric ratios with carbonate ions (Fig. 6A).

$NaHCO_3$-waters tend to be generally located close to tectonic alignments or contacts (e.g., Cortecci et al. 1999; Marini et al., 2000; Toscani et al., 2001; Venturelli et al., 2003) and their origin may be related to two main processes: (a) prograde Na-Ca ionic exchange (Toscani et al., 2001; Duchi et al., 2005), involving Na-rich clay releasing Na and acquiring Ca and Mg (Elliot et al., 1999; Venturelli et al., 2000; 2003); (b) prograde and long-lasting interaction and dissolution of plagioclase-rich silicate phases (Marini et al., 2000; Toscani et al. 2001), in conditions of saturation/oversaturation for carbonate-bearing minerals, that can favor the removal of Ca (and, secondarily, Mg and Sr).

Cation exchange reactions in the presence of clay minerals may affect the geochemistry of the *Group B* waters even considering that clay minerals are widely diffuse into the fluvio-lacustrine and alluvial deposits of MIB (Benvenuti, 1995, 1997). This hypothesis cannot however explain the relatively high contents of Li, B, and F detected for Na-HCO_3 waters as well as the high pH values. Many authors indeed suggested that prolonged interaction and dissolution of silicate mineral phases represent the main process governing the geochemical composition of Na-HCO_3 waters, with minor or even undetectable contributions due to cationic exchange reactions (Toscani et al., 2001; Venturelli et al., 2003). Long-lasting interactions between meteoric waters and feldspars (e.g., albite) generate alkaline hydrolysis reactions, releasing OH^- into the solution and thus leading to a considerable pH and Na increase, according to the reaction:

$$2NaAlSi_3O_8 + 11H_2O \rightarrow 2Na^+ + 2OH^- + 4H_4SiO_4 + Al_2Si_2O_5(OH)_4$$

Silicate dissolution as the predominant process allows to explain the relatively high concentrations of Li, B, and F. The fluoride enrichment in the *Group B* waters likely results from reactions involving silicate rocks containing F-bearing minerals such as apatite and fluorite, as suggested by Toscani et al. (2001) and supported by the correlation between F and Na (Tables 2 and 3). Boron and Li show a particular geochemical affinity with silicate mineral phases and thus, tend to be present in silicate rocks in considerable amounts (Leeman and Sisson, 1996). A positive correlation between the increase of B/Cl ratios (ranging within 31-48 and 0.7-4.6 for *Group B* and *A*, respectively) and Na can be highlighted in Fig. 8, thus suggesting boron increases as a consequence of silicate dissolution. Boron may also be adsorbed by several minerals in the fine-grained fraction of sediments and organic matter (Singh and Mattigod, 1992; Leeman and Sisson, 1996), resulting in an increase of the B/Cl ratio once interacting with the circulating waters. A similar behavior is detected for Li,

the average Li concentration in the *Group A* waters is about 8 μg/L, whilst for the *Group B* waters is ten times higher (≃80 μg/L).

The log(aNa^+/aH^+) vs. log(aH_3SiO_4) activity diagram is reported in Fig. 9. The *Group B* waters tend to be distributed along the equilibrium line of the albite and gibbsite stability fields (Bowers et al., 1984), thus indicating an equilibrium between the aqueous solution and both minerals. This would support the hypothesis that silicate dissolution is the main process influencing their composition, consequently cation exchange processes might have only a minor control on cation composition of this group of waters.

5.2 Dissolved gases geochemistry

As previously mentioned, the dissolved gases belonging to the waters of *Group A* are dominated by N_2 (relative abundance higher than 95%) and depleted in C-bearing compounds, whilst the *Group B* waters, though dominated by N_2 show considerable enrichments in CO_2 (up to 9 % v/v) and CH_4 (up to 61 % v/v), the latter becoming the major component in the BAG and PAN-S samples.

The most likely origin for N_2 (as well as for O_2 and Ar) is represented by the dissolution of atmospheric gases, as evidenced in the Ar-O_2-N_2 ternary plot (Fig. 10), where the sample distribution follows the alignment between two end-members: O_2-depleted reducing component and a superficial one with a composition similar to that of ASW (Air Saturated Water) (e.g., Giggenbach et al., 1983). Dissolution of atmospheric gases is particularly evident for the *Group A* waters whereas those pertaining to Group *B* show a strong O_2 depletion, as expected according to the negative Eh values measured in these waters (Table 2). Additionally, the N_2/Ar ratios for the investigated samples are indeed included within the ASW-domain, being comprised between 38 and 42. The influence of atmospheric gases in the MIB aquifers is evident when the $^4He/^{20}Ne$ ratios are considered as they are varying between 0.33 and 1.99 (Fig. 4). This evidence is also confirmed by the $^{40}Ar/^{36}Ar$ values (Table 4) as they approach the typical atmospheric signature ($^{40}Ar/^{36}Ar$ = 298.6; Lee et al., 2006).

The $\delta^{13}C$-CO_2 values showed relatively negative values and a large variability. According to the sample distribution (Fig. 11), the most probable origin of CO_2 was represented by plant-root respiration and/or anaerobic decay of organic matter trapped in the sediments, since these processes typically produce CO_2 with an isotopic signature comparable to that characterizing the MIB dissolved gases (Cerling et al., 1991; Whiticar, 1999), according to the following reactions:

(1) $C_6H_{12}O_6 + O_2 \rightarrow CO_2 + H_2O$ + heat energy (*plant respiration reaction*)

(2) $CH_2O + O_2 \rightarrow CO_2 + H_2O$ (*process of oxidation by dissolved O_2*)

(3) $2CH_2O + SO_4^{2-} + 2H^+ \rightarrow 2CO_2 + H_2S + 2H_2O$ (*process of oxidation by dissolved S^{6+}*)

where CH_2O is used as a simplified representation of organic matter. Considering pH-Eh conditions and oxygen fugacity, it is possible to assume that the CO_2 production is mostly controlled by reactions (1) and (2) for *Group A* and by reaction (3) for *Group B*, although the occurrence of additional processes able to influence the $\delta^{13}C$-CO_2 values cannot be ruled out (Venturi et al., 2017). Two samples (i.e., SAG and PI-P) are

characterized by less negative $\delta^{13}C\text{-}CO_2$ values (> -15 ‰ V-PDB) suggesting secondary CO_2 consumption processes (e.g., reduction). Moreover, the excess in dissolved (bi)carbonate species detected for the waters of *Group B* is likely to be related to the addition of CO_2 produced by reaction (3) (Cortecci et al., 1999). The occurrence of reaction (3) may also be held accountable for the presence of H_2S, which was not analytically determined but clearly smelt at the emergencies of the springs belonging to *Group B*.

As far as CH_4 is concerned, the most likely origin is represented by the decay of organic matter, although the wide variability of the $\delta^{13}C\text{-}CH_4$ values strongly supports the influence of secondary processes. In detail, waters from *Group A*, characterized by positive Eh values, are affected by microbial oxidation of biogenic CH_4 probably mediated by the activity of methanotrophic organisms (Whiticar, 1999) thus, causing isotopic fractionation with the production of residual CH_4 enriched in the heavier isotope.

Helium isotopes are useful to evaluate the possible interplay between deep-originated fluids and shallow aquifers (e.g., O'Nions and Oxburgh, 1988; Minissale et al., 2000; Minissale, 2004; Rizzo et al., 2015a, 2015b, 2016; Boudoire et al., 2020). The crustal production of ^4He via U and Th decay is assumed for R/R_a values ranging between 0.005-0.02 (Andrews, 1985), while the presence of mantle-deriving ^3He is generally accepted for values higher than 0.02 (Marty et al., 1992). It is worth noting that samples characterized by $^4He/^{20}Ne$ values approximating those in air ($^4He/^{20}Ne$=0.318) or ASW ($^4He/^{20}Ne$=0.285) do not produce reliable $^3He/^4He$ values once corrected for the presence of an atmospheric component. Consequently, the resulting R_c/R_a values yield an overestimation in the mantle contribution (Inguaggiato and Rizzo, 2004). However, only gas samples with $^4He/^{20}Ne > 1$ can thus be regarded to produce reliable air-corrected R_c/R_a values (Inguaggiato and Rizzo, 2004; Capasso et al., 2005). The MIB dissolved gases with $^4He/^{20}Ne > 1$ show R_c/R_a values between 0.07 and 0.38, with no significant differences between the waters of *Group A* and *Group B*. The R_c/R_a values higher than 0.1 can thus be considered anomalous for MIB, according to previous investigations on the $^3He/^4He$ in gas emissions from central-northern Italy (Minissale, 2004 and references therein). Therefore, the contribution from fluids deriving from mantle/magma degassing can be calculated according to the following equation:

$$M_c = [(R_c/R_a)_{sample} / (R_c/R_a)_{mantle}] \times 100$$

where M_c indicates *mantle (or magmatic) contribution*, (R_c/R_a)-sample is the $^3He/^4He$ measured for each sample and (R_c/R_a)-mantle indicates the hypothetical $^3He/^4He$ ratio for local mantle/magmatic end-member. Depending on the selected $^3He/^4He$ value as mantle/magmatic end-member, the respective percentage may vary significantly. Considering the European subcontinental lithospheric mantle average composition (R/R_a~6.5) (e.g., Guatheron et al., 2004), the obtained results show a contribution by the mantle/magmatic end-member of ~1-6%. Therefore, a weak, though present, input of mantle He can be envisaged in the MIB waters despite the fact that the geological-tectonic-geodynamical setting of the MIB is characterized by a thick-continental crust and an average geothermal gradient (Martini and Sagri, 1993). Nevertheless, MIB is thus apparently affected by active fault systems that favor the uprise of a mantle signature located at unknown

depth, suggesting important implications in terms of geochemical monitoring to assess the local seismic activity.

6. Insights into earthquake forecast and concluding remarks

A detailed geochemical characterization is fundamental for identifying the most useful and suitable geochemical parameters as possible seismic tracers for a given area. The results obtained by the water and dissolved gas geochemistry in the seismically active area of the Mugello Basin can be regarded as background values prior to future earthquake and the basis for deploying a geochemical monitoring network. According to our study, the investigated waters can be referred to a circulation at shallow depths although the helium isotopes have ascertained that a deep mantle-derived contribution cannot be considered negligible.

The geochemical monitoring should mainly be focused on those springs and shallow wells (*Group A*) located close to fault systems responsible for the recent seismic activity and/or that were active during and subsequently to the Quaternary (Delle Donne, 2005; Sani et al., 2009). A special focus should be dedicated to sulfur springs (*Group B*), since their emergence at surface is generally favored by the local structurers (i.e., faults, tectonic alignments). They are indeed generally associated with relatively prolongated and deep circulation patterns (Toscani et al., 2001; Venturelli et al., 2003), and are those showing the most relevant contribution by mantle fluids.

Summarizing, the analyzed waters have a meteoric origin and their composition is mainly controlled by water-rock interaction processes at low temperatures with carbonate- and silicate-bearing rocks. Moreover, since the isotopic composition of dissolved gases clearly shows an origin related to the dissolution of atmospheric and/or biogenic-derived gases, an uprising of deep crustal fluids under increasing seismic deformative and fracturing processes (e.g., Italiano et al., 2004; Bonfanti et al., 2012) may result in significant variations in both the chemical and isotopic gas composition, e.g. inputs of ^{3}He-rich gas may determine an increase in R/R_a (associated with higher $^{4}He/^{20}Ne$ ratios) and less negative $\delta^{13}C\text{-}CO_2$ values (e.g., Italiano et al., 2001). However, changes in major ion concentrations (i.e., Cl, SO_4) as well as in trace element contents (e.g., B, As, Fe) cannot be excluded. Nevertheless, additional hydrological and geochemical parameters are expected to be considered in future monitoring surveys, such as spring flow rates and well water levels, as observed during and after the 1919 Vicchio earthquake, and Rn concentrations, respectively.

Declaration of Competing Interests

The authors declare that they have no known competing financial interests or personal relationships that could have appeared to influence the work reported in this paper.

Acknowledgments

This study was financially supported by the Laboratory of Fluid and Rock Geochemistry of the Department of Earth Sciences at the University of Florence. The authors thank S. Venturi, G. Bicocchi and M. Lazzaroni for their assistance during part of the geochemical analyses. G. Corti and M. Taussi are warmly acknowledged for their support during the fieldwork and for some graphical restitution, respectively. We are finally grateful to M. Tantillo for helping in noble gas isotopic measurement and to INGV Sezione di Palermo for the help provided in the He and Ar isotopic analysis.

CRediT author statement

All authors contributed to the study and manuscript. **LC**: conceptualization, methodology, validation, formal analysis, investigation, data curation, writing – original draft; **JC**: conceptualization, methodology, validation, investigation, writing – original draft; **FT**: conceptualization, methodology, validation, investigation, writing – review and editing, supervision, project administration; **FC**: methodology, validation, investigation, writing – review and editing; **AR**: investigation, writing – review and editing; **SC**: investigation, writing – review and editing; **OV**: conceptualization, methodology, investigation, resources, supervision, project administration, writing – review and editing. All authors have approved the final version of the article.

References

Andrews, J. N., 1985. The isotopic composition of radiogenic helium and its use to study groundwater movements in confined aquifers. Chemical Geology, 49, 339-351, 10.1016/0009-2541(85)90166-4.

Barberio, M. D., Barbieri, M., Billi, A., Doglioni, C., Petitta, M., 2017. Hydrogeochemical changes before and during the 2016 Amatrice-Norcia seismic sequence (central Italy). Scientific Reports, 7 (1), 11735, https://doi.org/10.1038/s41598-017-11990-8.

Barbieri, M., Boschetti, T., Barberio, M. D., Billi, A., Franchini, S., Iacumin, P., Selmo, E., Petitta, M., 2020. Tracing deep fluid source contribution to groundwater in an active seismic area (Central Italy): a combined geothermometric and isotopic ($\delta^{13}C$) perspective. Journal of Hydrology, 582, 124495, https://doi.org/10.1016/j.jhydrol.2019.124495.

Barth, J. A. C., Cronin, A. A., Dunlop, J., Kalin, R. M., 2003. Influence of carbonates on riverine carbon cycle in an anthropogenically dominated catchment basin: evidence for major elements and stable carbon isotopes in the Lagan River (N. Ireland). Chemical Geology, 200, 203-216.

Benvenuti, M., 1995. Il controllo strutturale nei bacini intermontani Plio-Pleistocenici dell'Appennino Settentrionale: l'esempio della successione fluvio-lacustre del Mugello (Firenze). Il Quaternario, 8 (1), 53-60.

Benvenuti, M., 1997. – Physical stratigraphy of the fluvio-lacustrine Mugello Basin (Plio-Pleistocene, Northern Apennines, Italy). Giornale di Geologia, 59 (1/2), 91-111.

Benvenuti, M., 2003. Facies analysis and tectonic significance of lacustrine fan-deltaic successions in the Pliocene-Pleistocene Mugello Basin, Central Italy. Sedimentary Geology, 157, 197-234, 10.1016/S0037-0738(02)00234-8.

Benvenuti, M., Papini, M., 1997. Depositi continentali Plio-Pleistocenici nell'area di Monte Giovi. Relazione tra l'evoluzione idrografica e neotettonica della Valdisieve (Firenze). Il Quaternario, 10 (1), 105-120.

Boccaletti, M., Bonini, M., Moratti, G., Sani F., 1999. Compressive Neogene-Quaternary tectonics in the hinterland area of the Northern Apennines. Journal of Petroleum Geology, 22 (4), 37-60, https://doi.org/10.1111/j.1747-5457.1999.tb00458.x.

Boudoire, G., Rizzo, A. L., Di Muro, A., 2020. Paroxysmal eruptions tracked by variations of helium isotopes: inferences from Piton de la Fournaise (La Reunion Island). Scientific Reports, 10, 9809.

Bonfanti, P., Genzano, N., Heinicke, J., Italiano, F., Martinelli, G., Pergola, N., Telesca, L., Tramutoli, V., 2012. Evidence of CO_2-gas emission variations in the Central Apennines (Italy) during L'Aquila seismic sequence (March-April 2009). Bollettino di Geofisica Teorica ed Applicata, 53, 147-169.

Bonini, M., Corti, G., Delle Donne, D., Sani, F., Piccardi, L., Vannucci, G., Genco, R., Martelli, L., Ripepe, M., 2016. Seismic sources and stress transfer interaction among axial normal faults and external thrust fronts in the Northern Apennines (Italy): a working hypothesis based on the 1916-1920 time-space cluster of earthquakes. Tectonophysics, 680, 67-89, https://dx.doi.org/10.1016/j.tecto.2016.04.045.

Bortolotti, V., Poccianti, C., Principi, G., Sani, F., 2010. Note Illustrative della Carta Geologica d'Italia alla scala 1:50000. Foglio 264 Borgo San Lorenzo. Serv. Geol. d'It-Università degli Studi di Firenze.

Boschetti, T., Barbieri, M., Barberio, M. D., Billi, A., Franchini, S., Petitta, M., 2019. Geochemistry, Geophysics, Geosystems, 20, 2303-2317, https://doi.org/10.1029/2018GC008117.

Bowers, T. S., Jackson, K. J., Helgeson, H. C., 1984. Equilibrium activity diagrams: for coexisting minerals and aqueous solutions at pressures and temperatures to 5 kb and 600°C. Springer-Verlag,

Capaccioni, B., Vaselli, O., Moretti, E., Tassi, F., Franchi, R., 2003. The origin of thermal waters from the eastern flank of the Dead Sea Rift Valley (western Jordan). Terra Nova, 15, 145-154.

Capasso, G., Inguaggiato, S., 1998. A simple method for the determination of dissolved gasses in natural waters. An application to thermal waters from Volcano Island. Applied Geochemistry, 13 (5), 631-642, https://doi.org/10.1016/S0883-2927(97)00109-1.

Capasso, G., Carapezza, M. L., Federico, C., Inguaggiato, S., & Rizzo, A., 2005. Geochemical monitoring of the 2002–2003 eruption at Stromboli volcano (Italy): Precursory changes in the carbon and helium isotopic composition of fumarole gases and thermal waters. Bulletin of Volcanology, 68(2), 118–134. https://doi.org/10.1007/s00445-005-0427-5

Center for Research on the Epidemiology of Disaster (CRED), 2015. The Human Cost of Natural Disasters: a global perspective. CRED-Institute of Health and Society (IRSS)-The United Nation Offices for Disaster Risk Reduction (UNISDR).

519 Cerling, T. E., Solomon, D. K., Quade, J., Bowman, J. R., 1991. On the isotopic composition of carbon in soil
520 carbon dioxide. Geochim. Cosmochim. Acta, 55, 3403-3405, https://doi.org/10.1016/0016-
521 7037(91)90498-T.
522 Cicerone, R. D., Ebel, E. J., Britton, J., 2009. A systematic compilation of earthquake precursors.
523 Tectonophysics, 476 (3-4), 371-396, https://doi.org/10.1016/j.tecto.2009.06.008.
524 Claesson, L., Skelton, A., Graham, C., Dieti, C., Mörth, C-M., Torssander, P., Kockum, I., 2004.
525 Hydrogeochemical changes before and after a major earthquake. Geology, 32, 641-644,
526 https://doi.org/10.1130/G20542.1.
527 Conti, P., Cornamusini, G., Carmignani, L., 2020. An outline of the geology of the Northern Apennines (Italy),
528 with geological map 1:250.000 scale. Ital. J. Geosci., 139, 149-194.
529 Cortecci, G., Calafato, A., Boschetti, T., 1999. New chemical and isotopic data on the groundwater system of
530 Bagno di Romagna, northern Apennines, Emilia-Romagna province, Italy. Miner. Petrog. Acta, XLII,
531 89-101.
532 Craig, H., 1961. Isotopic variations in meteoric waters. Science, 133, 1702-1703.
533 Delle Donne, D., 2005. Tettonica attiva dell'Appennino Settentrionale nel settore compreso tra l'Appennino
534 Pistoiese e l'alta Val Tiberina. PhD Thesis. University of Florence, 144 pp.
535 DISS Working Group, 2021. Database of individual seismogenic sources (DISS), Version 3.3.0: A compilation
536 of potential sources for earthquakes larger than M 5.5 in Italy and surroundings area. Istituto Nazionale
537 di Geofisica e Vulcanologia (INGV), https://doi.org/10.13127/diss3.3.0.
538 Duchi, V., Venturelli, G., Boccasavia, I., Bonicolini, F., Ferrari, C., Poli, D., 2005. Studio geochimico dei
539 fluidi dell'Appennino Tosco-Emiliano-Romagnolo. Bollettino della Società Geologica Italiana, 124,
540 475-491.
541 Elliot, T., Andrews, J. N., Edmunds, W. N., 1999. Hydrochemical trends, paleorecharge and groundwater ages
542 in the fissured Chalk aquifer of the London and Berkshire basins, UK. Applied Geochemistry, 14, 333-
543 363, 10.1016/S0883-2927(98)00060-2.
544 Franchini, S., Agostini, A., Barberio, M. D., Barbieri, M., Billi, A., Boschetti, T., Pennisi, M., Petitta, M.,
545 2020. HydroQuakes, central Apennines, Italy: towards a geochemical monitoring network for seismic
546 precursors and the hydro-seismo-sensitivity of boron, Journal of Hydrology, 598, 1-16.
547 10.1016/j.jhydrol.2020.125754
548 Gat, J.R., Carmi, H. 1970. Evolution of isotopic composition of atmospheric waters in the Mediterranean Sea
549 area. J. Geophys. Res., 75, 3039-3040.
550 Gautheron, C., Moreira, M., Allègre, C., 2004. He, Ne and Ar composition of the European lithospheric mantle.
551 Chemical Geology, 217 (1-2), 97-112, 10.1016/j.chemgeo.2004.12.009.
552 Gibbs, R. J., 1970. Mechanisms controlling world water chemistry. Science, 170, 1088-1090.
553 Giustini, F., Brilli, M., Patera, A., 2016. Mapping oxygen stable isotopes of precipitation in Italy. J. Hydrol.
554 Regional Studies, 8, 162-181.

555 Giggenbach, W. F., Gonfiantini, R., Jangi, B. L., Truesdell, A. H., 1983. Isotopic and chemical composition
556 of Parbaty Valley geothermal discharges, NW-Himalaya. Geothermics, 12, 199-222.
557 Gori, F., Barberio, M. D., 2022. Hydrogeochemical changes before and during the 2019 Benevento seismic
558 swarn in central-southern Italy. Journal of Hydrology, 604, 127250,
559 https://doi.org/10.1016/j.jhydrol.2021.127250
560 Hosono, T., Yamada, C., Shibata, T., Tawara, Y., Wang, C-Y., Manga, M., Rahman, A. T. M. S., Shimada, J.,
561 2019. Coseismic groundwater drawdown along crustal ruptures during the 2016 M_w 7.0 Kumamoto
562 earthquake. Water Resource Research, 55, 5891-5903, https://doi.org/10.1029/2019WR024871.
563 Inguaggiato, S., Rizzo, A., 2004. Dissolved helium isotope ratios in ground-waters: a new technique based on
564 gas-water re-equilibration and its application to Stromboli volcanic system. Applied Geochemistry, 19,
565 665-673, https://doi.org/10.1016/j.apgeochem.2003.10.009.
566 Italiano, F., Martinelli, G., Nuccio, P. M., 2001. Anomalies of mantle-derived helium during the 1997-1998
567 seismic swarm of Umbria-Marche, Italy. Geophysical Research Letters, 28, 839-842.
568 Italiano, F., Martinelli, G., Rizzo, A., 2004. Geochemical evidence of seismogenic-induced anomalies in the
569 dissolved gases of thermal waters: A case of study of Umbria (Central Apennines, Italy) both during
570 and after the 1997-1998 seismic swarm. Geochemistry, Geophysics, Geosystems, Vol. 5,
571 https://doi.org/10.1029/2004GC000720.
572 Jeelani, G., Bhat, N. A., Shivanna, K., Bhat, M. Y., 2011. Geochemical characterization of surface water and
573 spring water in SE Kashmir Valley, western Himalaya: implications to water-rock interaction. J. Earth
574 Syst. Sci., 120, 921-932.
575 Lee, J-Y., Marti, K., Severinghaus, J. P., Kawamura, K., Yoo, H. S., Lee, J. B., Kim, J. S., 2006. A
576 redetermination of the isotopic abundances of atmospheric Ar. Geochim. Cosmochim. Acta, 70, 4507-
577 4512. http://dx.doi.org/10.1016/j.gca.2006.06.1563.
578 Leeman, W. P., Sisson, V. B., 1996. Geochemistry of boron and its implications for crustal and mantle
579 processes. In: Grew, E. S., Anovitz, L. M., (Eds), Boron: mineralogy, petrology and geochemistry,
580 Review in Mineralogy, 33, 645-707.
581 Longinelli, A., Selmo, E., 2003. Isotopic composition of precipitation in Italy: a first overall map. J. Hydrol.,
582 270, 75-88, https://doi.org/10.1016/S0022-1694(02)00281-0.
583 Mamyrin, B. A., Tolstikhin, I. N., 1984. Helium isotopes in nature. Elsevier. Amsterdam.
584 Marini, L., Ottonello, G., Canepa, M., Cipolli, F., 2000. Water-rock interaction in the Bisagno Valley (Genoa,
585 Italy): application of an inverse approach to model spring water chemistry. Geochimica et
586 Cosmochimica Acta, 64 (15), 2617-2635, 10.1016/S0016-7037(00)00383-5.
587 Martinelli, G., 2000. Contribution to a history of earthquake prediction research. Seismological Research
588 Letters, 71 (5), 583-588. https://doi.org/10.1785/gssrl.71.5.583.
589 Martinelli, G., 2020. Previous, current and future trends in research into earthquake precursors in geofluids.
590 Geosciences, 10 (5), 189, https://doi.org/10.3390/geosciences10050189.

Martinelli, G., Minissale, A., Verrucchi, C., 1998. Geochemistry of heavily exploited aquifers in the Emilia-Romagna region (Po Valley, northern Italy). Environmental Geology, 36, 195-206. https://doi.org/10.1007/s002540050335.

Martini, I. P., Sagri, M., 1993. Tectono-sedimentary characteristics of the late Miocene-Quaternary extensional basins of the Northern Apennines, Italy. Earth Science Reviews, 34, 197-233, https://doi.org/10.1016/0012-8252(93)90034-5.

Marty, B., O'Nions, R. K., Oxburgh, E. R., Martel, D., Lombardi, S., 1992. Helium isotopes in Alpine regions. Tectonophysics, 206, 71-78, https://doi.org/10.1016/0040-1951(92)90368-G.

Merritt, D. A., Hayes, J. M., Des Marais, D. J., 1995. Carbon isotopic analysis of atmospheric methane by isotope-ratio-monitoring gas chromatography-mass spectrometry. Journal Geophysical Research, 100D1, 1317-1326, 10.1029/94jd02689.

Minissale, A., Magro, G., Martinelli, G., Vaselli, O., Tassi F., 2000. Fluid geochemical transect in the Northern Apennines (central-northern Italy): fluid genesis and migration and tectonic implications. Tectonophysics, 319, 199-222, https://doi.org/10.1016/S0040-1951(00)00031-7.

Minissale, A., 2004. Origin, transport and discharge of CO_2 in central Italy. Earth-Science Reviews, 66 (1-2), 89-141.

Minissale, A., Vaselli, O., 2011. Karst spring as "natural" pluviometers: constraints on the isotopic composition of rainfall in the Apennines of central Italy, Applied Geochemistry, 26 (5), 838-852, https://doi.org/10.1016/j.apgeochem.2011.02.005.

Natali, S., Doveri, M., Giannecchini, R., Baneschi, I., Zanchetta, G., 2022. Is deuterium excess in precipation a reliable tracers of moisture sources and water resources fate in the western Mediterranean? New insights from Apuan Alps (Italy). J. Hydrol., 614, 128497.

Nisi, B., Raco, B., Dotsika, E., 2014. Groundwater contamination studies by environmental isotopes: a review. In: AA. VV. (Eds), Environment, Energy and Climate Change I: Environmental Chemistry of Pollutants and Wastes.

O'Nions, R. K., Oxburgh, E. R., 1988. Helium, volatile fluxes and the development of continental crust. Earth Planet Sci. Lett., 90, 331-347, https://doi.org/10.1016/0012-821X(88)90134-3.

Parkhust, D. L., Appelo, C. A., 1999. User's guide to PHREEQC (version 2). A computer program for speciation, batch-reactions, one-dimensional transport, and inverse geochemical calculations. US Geological Survey, Water-Resources Investigation Report 95-4259, Denver, Colorado.

Poreda, R. J., Craig, H., 1989. Helium isotope ratios in circum-Pacific volcanic arcs. Nature, 338, 473-478,

Reddy, D. V., Kumar, D., Rao, P. N., 2017. Long-term hydrogeochemical earthquake precursors studies at Konya-Warna reservoir site in Western India. Journal of the Geological Society of India, 90, 720-727, 10.1007/s12594-017-0781-x.

Rizzo, A. L., Barberi, F., Carapezza, M. L., Di Piazza, A., Francalanci, L., Sortino, F., D'Alessandro, W., 2015a. New magma refilling a quiescent volcano: Evidence from He-Ne-Ar isotopes during the 2011-2012 unrest at Santorini, Greece. Geochemistry, Geophysics, Geosystems, March 2015, 798-814.

628 Rizzo, A. L., Federico, C., Inguaggiato, S., Sollami, A., Tantillo, M., Vita, F., Bellomo, S., Longo, M., Grassa,
629 F., Liuzzo, M., 2015b. The 2014 effusive eruption at Stromboli volcano (Italy): Inferences from soil
630 CO_2 flux and $^3He/^4He$ ratio in thermal waters. Geophysical Research Letters, 42(7), 2235–2243.
631 https://doi.org/10.1002/2014GL062955.
632 Rizzo, A. L., Caracausi, A., Chavagnac, V., Nomikou, P., Polymenakou, P., Mandalakis, M., Kotoulas, G.,
633 Magoulas, A., Castillo, A., Lampridou, D., 2016. Kolumbo submarine volcano (Greece):An active
634 window into the Aegean subduction system. Scientific Reports, 6(1), 28013.
635 Rodolfi, G., 2006. Valutazione del danno subito dalle risorse idriche. In: AA. VV., Valutazione del danno
636 ambientale conseguente ai lavori per la realizzazione della ferrovia ad alta velocità Milano-Napoli
637 (Tratto in territorio toscano tra Firenze e Bologna). Processo CAVET, 83 pp.
638 Rovida, A., Locati, M., Camassi, R., Lolli, B., Gasperini, P., 2020. The italian eartquake catalogue CPTI15.
639 Bulletin of Earthquake Engineering, 18 (7), 2953-2984, doi:10.1007/s10518-020-00818-y.
640 Rovida, A., Locati, M., Camassi, R., Lolli, B., Gasperini, P., Antonucci, A., 2021. Catalogo parametrico dei
641 terremoti italiani (CPTI15), versione 3.0. Italy: Instituto Nazionale di Geofisica e Vulcanologia INGV.
642 Saccorotti, G., Bruni, R., Bonini, M., Corti, G., Keir, D., Sani, F., 2022. Recent seismic sequences and
643 activation of normal fault systems in the Mugello Basin and surrounding areas (Northern Apennines,
644 Italy). Frontiers in Earth Science, 10;879160, https://doi.org/10.3389/feart.2022.879160.
645 Sani, F., Bonini, M., Piccardi, L., Vannucci, G., Delle Donne, D., Benvenuti, M., Moratti, G., Corti, G.,
646 Montanari, D., Sedda, L., Tanini, C., 2009. – Late Pliocene-Quaternary evolution of outermost
647 hinterland basins of the Northern Apennines (Italy) and their relevance to active tectonics.
648 Tectonophysics, 476, 336-356, https://doi.org/10.1016/j.tecto.2008.12.012.
649 Sciarra, A., Cantucci, B., Coltorti, M., 2017. Learning from soil gas change and isotopic signatures during
650 2012 Emilia seismic sequence. Scientific Reports, 7, 14187.
651 Sestini, G., 1970. Postgeosynclinal deposition. In: Sestini, G., (Eds.), Development of the Northern Apennines
652 Geosyncline. Sedimentary Geology, 4, 481-520.
653 Singh, S. P. N., Mattigod, S. V., 1992. Modelling of boron adsorption on kaolinite. Clay and clay minerals,
654 40, 192-205.
655 Skelton, A., Andrén, M., Kristmannsdóttir, H., Stockmann, G., Mörth, C-M., Sveinbjörnsdòttir, A., Jónsson
656 S., Sturkell, E., Guorúnardóttir, H-R., Hjartarson, H., Siegmund, H., Kockum, I., 2014. Changes in
657 groundwater chemistry before two consecutive earthquakes in Iceland, Nature Geoscience, 7, 752,
658 https://doi.org/10.1038/ngeo2250.
659 Skelton, A., Claesson, L., Wästeby, N., Andrén, M., Stockmann, G., Sturkell, E., Mörth, C-M., Stefansson,
660 A., Tollefsen, E., Siegmund, H., Keller, N., Kjartansdóttir, R., Hjartarson, H., Kockum, I., 2019.
661 Hydrogeochemical changes before and after earthquakes based on long-term measurements of multiple
662 parameters at two sistes in Northern Iceland – a review. Journal of Geophysical Research: Solid Earth,
663 124, 2702-2720, https://doi.org/10.1029/2018JB016757.
664 Tassi, F., Vaselli, O., Tedesco, G., Montegrossi, G., Darrah, T., Cuoco, E., Mapendano, M. Y., Poreda, R.,
665 Delgado-Huertas, A., 2009. Water and gas chemistry at Lake Kivu (DRC): Geochemical evidences of

vertical and horizontal heterogeneities in a multibasin structure. Geochemistry, Geophysics, Geosystems, 10, 1-12.

Thomas, D., 1988. Geochemical precursors to seismic activity. Pure and Applied Geophysics, 126, 241-266, http://dx.doi.org/10.1007/BF00878998.

Torres-Martínez, J. A., Mora, A., Knappett, P. S. K., Ornelas-Sotos, N., Mahlknecht, J., 2020. Tracking nitrate and sulfate sources in groundwater of an urbanized valley using a multi-tracer approach combined with a Bayesian isotope mixing model. Water Res., 182, 115962.

Torres-Martínez, J. A., Mora, A., Mahlknecht, J., Daesslé, L. W., Cervantes-Avilés, P. A., Ledesma-Ruiz, R., 2021. Estimation of nitrate pollution sources and transformations in groundwater of an intense livestock-agricultural area (Comarca, Lagunera), combining major ions, stable isotopes and MixSTAR model. Enviro. Pollut,, 269, 115445.

Toscani, L., Venturelli, G., Boschetti, T., 2001. Sulphide-bearing waters in Northern Apennines, Italy: general features and water-rock interaction. Applied Geochemistry, 7, 195-216, 10.1023/A:1012941328028.

Vai, G., 2001. Structure and stratigraphy: an overview. In: Vai, G., Martini, I. P., (Eds.), Anatomy of an Orogen: The Apennines and the Adjacent Mediterranean Basins. Kluwer Academic Publishing Dordrecht, 15- 31.

Vaselli, O., Tassi, F., Montegrossi, G., Capaccioni, B., Giannini, L., 2006. Sampling and analysis of volcanic gasses. Acta Vulcanologia, 18, 65-76.

Venturelli, G., Boschetti, T., Duchi, V., 2003. Na-carbonate waters of extreme composition: possible origin and evolution. Geochemical Journal, 37, 351-366, https://doi.org/10.2343/geochemj.37.351.

Venturelli, G., Toscani, L., Mucchino, C., Voltolini C., 2000. Study of water-rock interaction of spring waters in the north-Apennines. Annali di Chimica, 90, 359-368.

Venturi, S., Tassi, F., Bicocchi, G., Cabassi, J., Capecchiacci, F., Capasso, G., Vaselli, O., Ricci, A., Grassa, F., 2017. Fractionation processes affecting the stable carbon isotope signature of thermal waters from hydrothermal/volcanic systems: the examples of Campi Flegrei and Vulcano Island (southern Italy). Journal of Volcanology and Geothermal Research, 345, 46-57, doi.org/10.1016/j.jvolgeores.2017.08.001.

Vespasiano, G., Apollaro, C., De Rosa, R., Muto, F., Larosa, S., Fiebig, J., Mulch, A., Marini, L., 2015. The Small Spring Method (SSM) for the definition of the stable isotope-elevation relationships in northern Calabria (southern Italy). Applied Geochemistry, 63, 333-346, 10.1016/j.apgeochem.2015.10.001.

Wang, C-Y., Manga, M., 2021. Water and earthquakes. Springer Nature.

Whiticar, M. J., 1999. Carbon and hydrogen isotope systematics of bacterial formation and oxidation of methane. Chem. Geol., 161, 291-314, https://doi.org/10.1016/S0009-2541(99)00092-3.

Wilhelm, E., Battino, R., Wilcock, R. J., 1977. Low-pressure solubility of gasses in liquid waters. Chem. Rev., 77, 219-262, https://doi.org/10.1021/cr60306a003.

Tables

Table 1: Sampling points
Sample name and ID, type (s, cold spring; ss, sulfur spring; w, well; mv, mud volcano), geographic location (UTM-32T WGS 84 coordinates) and altitude (m a.s.l).

full name	ID	type	East (WGS84-UTM)	North (WGS84-UTM)	Altitude (m)
Acqualica	ACQ	s	684163	4878080	390
Bagnolo Sulfurea	BAG	ss	689957	4882062	652
Bartolacci (Fonte di Fabio)	BAR	s	687500	4863972	564
Bricciana	BRI	s	699140	4863070	306
Casaglia Sulfurea	CS-S	ss	701054	4879537	751
Casole Vicchio	CAS	s	699113	4868715	213
Castel del Trebbio	CdT	s	683542	4869333	436
Celle	CEL	s	702064	4861706	253
Cimitero Dicomano	CIM-D	s	702462	4863410	184
Cornocchio	COR	s	678000	4871042	305
Faltona	FAL	s	689501	4867548	336
Faltona2	FAL2	s	688451	4867533	256
Fonte del Castagno	FdC	s	695901	4876298	424
Fonte dell'Alpe	FdA	s	698513	4879376	860
Fonte dell'Ascensione	ASC	s	683113	4869644	402
Forese (Fonte Sant'Antonio)	FdSA	s	702877	4862485	155
Madonna dei Tre Fiumi	MTF	s	695900	4876597	429
Madonna del Vivavio	MdV	s	688680	4874107	277
Montui	MON	s	680397	4870346	389
Palazzuolo Solforosa	PAL	ss	703864	4887837	431
Panna	PAN	s	682940	4882272	572
Panna Sulfurea	PAN-S	ss	682932	4882281	572
Piandrati	PIA	s	703247	4861231	151
Piazzano Casa	PI-C	w	694446	4870954	223
Piazzano Pozzo	PI-P	w	694494	4870904	218
Piazzano Sorgente	PI-S	s	694372	4870709	224
Pieve Dicomano	PIE-D	s	702649	4863203	196
Ponte a Olmo	PaO	s	684504	4879876	502
Razzuolo (Fonte del Mulino)	R-FM	s	697521	4878117	623
Sagginale	SAG	ss	693199	4867122	200
San Gavino	S-GA	s	687472	4874428	264
San Giovanni	S-GV	s	681972	4871030	316
Santa Lucia	S-LU	s	681807	4883032	702
Strada Vecchia	SVE	s	702334	4862393	179
Tartufaia	TAR	ss	687815	4876435	293
Topo Scarperia	TOP	s	688227	4873922	250
Trebbio2	TR-2	s	683440	4868985	420
Trebbio3	TR-3	s	683477	4868756	432
Villore	VIL	s	703879	4871111	370
Vulcano Fango Monte	VFm	mv	694440	4870732	217
Vulcano Fango Valle	VFv	mv	694480	4870425	215

Table 2: Water characteristics and isotopic analysis

Water physicochemical parameters (pH, T in ºC and Eh in meV); major anions (HCO_3^-, CO_3^{2-}, Cl^-, NO_3^- and SO_4^{2-}), cations (Ca^{2+}, Mg^{2+}, Na^+, K^+), and total dissolved solids (TDS) are reported in mg/L. Water stable isotopes are expressed as V-SMOW ‰. (n.a. = not analyzed).

ID	pH	T	Eh	HCO_3^-	CO_3^{2-}	Cl^-	NO_3^-	SO_4^{2-}	Ca^{2+}	Mg^{2+}	Na^+	K^+	TDS	$\delta^{18}O$	$\delta^{2}H$
ACQ	7.33	14.3	243	265		35	0.5	11	51	26	10	0.7	408	-7.27	-44.1
BAG	9.40	12.5	-227	547	55.0	15	2.3	14	14	2	230	3.1	895	-7.97	-48.2
BAR	8.60	14.4	156	66	1.2	9	0.2	29	27	3	8	0.9	158	-7.50	-44.8
BRI	8.24	14.0	109	236		10	1.3	25	67	10	7	0.9	370	-7.30	-44.2
CS-S	9.68	14.6	-252	328	65.0	10	0.9	17	16	3	155	1.2	607	-8.20	-50.2
CAS	7.81	15.2	148	482		10	2.3	98	143	24	24	1.5	816	-6.23	-40.7
CdT	7.76	21.3	232	470		16	1.4	14	168	4	6	0.8	687	-7.13	-43.0
CEL	8.34	15.4	111	260	1.2	13	6.2	34	73	17	13	0.9	435	-6.83	-42.6
CIM-D	8.14	16.1	126	512		17	3.7	53	124	31	16	2.1	787	-6.51	-42.2
COR	8.75	16.3	213	244	6.3	10	7.5	17	74	12	10	1.6	387	-6.98	-42.6
FAL	7.96	15.8	141	415		13	2.1	21	116	10	11	0.5	601	-6.91	-43.3
FAL2	8.58	16.2	201	290	1.9	13	6.0	22	98	6	10	3.6	461	-6.98	-43.2
FdC	8.70	15.6	192	314	4.0	12	0.2	34	81	21	9	4.4	494	-7.64	-47.7
FdA	8.50	12.3	221	183	1.5	11	2.9	32	45	16	6	0.9	309	-8.13	-49.6
ASC	8.43	17.5	214	411	3.2	11	4.9	14	145	4	6	3.0	464	-7.08	-43.3
FdSA	8.28	16.9	110	318		13	12.9	37	86	13	19	2.3	517	-6.85	-43.5
MTF	8.60	16.0	172	272	2.7	12	1.0	49	66	22	10	2.9	452	-7.83	-47.6
MdV	7.77	16.2	146	402		36	53.8	49	119	24	35	2.1	740	-6.89	-44.1
MON	8.40	20.8	215	386	3.4	13	0.4	22	116	15	15	0.1	580	-6.86	-41.3
PAL	9.41	22.4	-183	502	58.2	13	0.4	26	12	2	219	2.4	848	-8.67	-56.6
PAN	8.51	15.3	110	233	1.9	9	0.3	34	59	16	12	0.4	380	-7.72	-46.9
PAN-S	8.95	14.6	-255	380	8.7	12	<0.1	10	7	2	140	1.7	570	-7.82	-46.9
PIA	8.04	18.7	129	362		15	3.3	87	90	33	20	3.2	635	-6.89	-43.8
PI-C	7.64	*25.3*	167	453		24	1.1	55	120	22	26	3.7	724	-7.04	-44.2
PI-P	7.95	17.2	-106	354		18	0.1	9	34	5	87	1.9	540	-8.05	-51.5
PI-S	7.87	20.6	115	512		17	58.0	26	155	19	15	2.7	819	-6.80	-43.8
PIE-D	8.00	19.0	128	408		17	2.1	54	110	27	14	2.1	659	-6.48	-42.0
PaO	7.48	15.6	202	293		12	1.3	30	81	12	11	1.7	455	-7.19	-44.2
R-FM	8.54	12.5	171	277	2.4	7	0.7	24	70	18	5	1.7	423	-7.98	-48.2
SAG	8.88	16.2	-182	429	8.3	25	<0.1	6	9	5	156	1.2	646	-7.42	-45.9
S-GA	8.75	17.2	153	338	4.8	19	39.8	39	121	11	11	2.1	602	-7.03	-44.6
S-GV	8.50	18.2	202	412	4.1	16	1.7	18	130	10	10	2.6	619	-6.98	-42.2
S-LU	8.35	15.0	229	310	1.5	11	2.8	33	96	15	8	1.5	499	-7.50	-45.9
SVE	8.08	16.1	118	430		20	15.0	29	125	8	20	3.9	662	-6.66	-42.2
TAR	8.66	16.5	-51	377	4.3	13	0.2	33	101	14	16	0.5	594	-7.11	-45.0
TOP	7.57	17.8	159	391		25	31.0	40	126	10	24	1.8	665	-6.93	-43.1
TR-2	8.27	14.0	246	390		12	1.4	14	141	4	6	0.7	576	-7.31	-43.9
TR-3	7.77	22.7	233	403		8	8.1	13	139	6	9	0.8	594	-6.95	-42.9
VIL	7.82	*23.0*	135	215		8	0.6	31	52	14	10	1.5	347	-8.29	-52.2
VFm	8.60	6.9	92	292		13	4.3	44	82	19	10	1.4	469	n.a.	n.a.
VFv	8.10	6.8	137	289		14	4.9	49	84	19	10	1.2	471	n.a.	n.a.

720 Table 3: Minor and trace elements
721 Minor elements (F^-, Br^-, NH_4^+ and SiO_2) are reported in mg/L Trace elements (Li, B, Fe, Mn, Sr and As) are reported in
722 µg/L. (n.a. = not analyzed).
723

ID	F^-	Br^-	NH_4^+	SiO_2	Li	B	Fe	Mn	Sr	As
ACQ	0.22	0.13	0.01	9.3	0.3	132	5	<1	79	<0.1
BAG	4.57	0.07	0.40	8.2	117	1050	31	<1	148	<0.1
BAR	0.27	0.04	0.03	9.8	1.4	8	<5	<1	48	<0.1
BRI	0.66	0.02	0.01	12.1	5.4	13	<5	<1	398	<0.1
CS-S	2.00	0.02	0.40	11.1	47.6	461	801	9.4	124	0.1
CAS	0.43	0.28	0.01	8.3	22.4	120	<5	<1	870	<0.1
CdT	0.01	0.05	0.04	16.4	1.6	13	<5	<1	370	<0.1
CEL	0.18	0.02	0.01	13.5	9.8	22	<5	<1	533	0.1
CIM-D	0.67	0.07	0.01	9.9	11.5	44	<5	<1	615	<0.1
COR	0.23	0.02	0.01	12.0	5.8	15	23	<1	263	0.1
FAL	1.21	0.10	0.01	9.5	5.4	16	<5	<1	555	<0.1
FAL2	0.01	0.04	0.01	10.0	3.1	21	21	<1	301	<0.1
FdC	0.14	0.03	0.03	7.2	7.2	20	7	<1	369	<0.1
FdA	0.16	0.02	0.03	7.6	5.2	15	<5	<1	232	<0.1
ASC	0.11	0.06	0.12	19.6	1.3	13	14	<1	341	<0.1
FdSA	0.23	0.06	0.01	9.6	7.2	29	<5	<1	560	0.2
MTF	0.55	0.01	0.03	22.0	8.4	36	<5	<1	793	0.1
MdV	0.25	0.10	0.03	8.2	11.8	47	<5	<1	436	0.2
MON	0.62	0.13	0.21	10.4	5.4	42	8	1.1	441	<0.1
PAL	1.87	0.10	0.51	10.2	28.5	725	10	<1	105	<0.1
PAN	0.17	0.01	0.01	11.1	10.7	32	<5	1.9	561	<0.1
PAN-S	1.41	0.02	0.46	15.2	90.0	555	8	1.8	358	<0.1
PIA	0.13	0.01	0.03	15.6	20.6	66	<5	<1	939	<0.1
PI-C	0.32	0.01	0.05	19.5	5.6	74	5	19.1	491	0.3
PI-P	0.23	0.03	8.06	12.7	5.2	248	191	68.2	193	5.5
PI-S	0.19	0.01	0.01	12.2	6	24	<5	2.1	490	0.1
PIE-D	0.15	0.07	0.03	8.1	10.7	58	<5	<1	1031	<0.1
PaO	0.43	0.03	0.03	6.7	5.8	58	<5	<1	587	0.1
R-FM	0.08	<0.01	0.01	11.2	5.2	15	<5	<1	281	<0.1
SAG	1.85	0.02	1.29	14.0	175	771	10	1.4	928	<0.1
S-GA	0.41	0.01	0.01	9.8	5.1	26	<5	<1	440	0.2
S-GV	0.73	0.15	0.05	8.3	3.1	29	5	1.5	484	<0.1
S-LU	0.38	0.17	<0.01	12.7	8.0	21	<5	<1	298	<0.1
SVE	0.27	0.15	0.01	19.8	3.8	23	<5	<1	535	<0.1
TAR	0.20	<0.01	0.85	12.8	5.8	38	305	209	529	<0.1
TOP	0.23	0.03	0.01	7.7	4.9	71	<5	<1	392	<0.1
TR-2	<0.01	0.02	0.05	7.8	1.7	13	<5	<1	314	<0.1
TR-3	<0.01	0.37	0.01	7.6	1.9	33	6	<1	327	<0.1
VIL	0.38	0.09	0.01	7.6	5.0	33	11	1.2	366	<0.1
VFm	0.23	0.01	0.04	7.4	6.2	25	5	3.5	453	0.2
VFv	0.19	0.01	0.08	19.0	5.9	24	5	4.1	439	0.2

724
725
726
727
728
729
730

Table 4: Dissolved gases chemical and isotopic composition

Chemical and isotopic composition of dissolved gases: CO_2, CH_4, N_2, O_2, Ar and He are reported in µmol/L; $\delta^{13}C\text{-}CO_2$ and $\delta^{13}C\text{-}CH_4$ are expressed as V-PDB ‰; $^3He/^4He$ expressed as R/R_a, $^4He/^{20}Ne$ and $^{40}Ar/^{36}Ar$ are also reported. For those samples with $^4He/^{20}Ne > 1$, $^3He/^4He$ were also reported as R_c/R_a. Errors (+/-) for R/R_a and $^{40}Ar/^{36}Ar$ are included. "n.d." indicates "not detected" due to the low methane concentration and "n.a." indicates not analyzed.

ID	CO_2	CH_4	N_2	O_2	Ar	He	$\delta^{13}C\text{-}CO_2$	$\delta^{13}C\text{-}CH_4$	R/R_a	R/R_a +/- error	R_c/R_a	$^4He/^{20}Ne$	$^{40}Ar/^{36}Ar$	$^{40}Ar/^{36}Ar$ +/- error
ACQ	11	0.01	754	131	18	0.010	-23	n.d.	n.a.	n.a.	n.a.	n.a.	n.a.	n.a.
BAG-S	65	585	448	26	19	0.013	-21	-64	0.35	0.000	0.07	1.06	302.2	0.0003
BAR	1.8	0.01	721	310	18	0.011	-22	n.d.	0.97	0.005	-	0.68	298.6	0.0001
BRI	16	0.01	809	236	20	0.011	-20.5	n.d.	0.94	0.004	-	0.81	301.2	0.0002
CS-S	55	95	715	31	18	0.012	-25	-65	n.a.	n.a.	n.a.	n.a.	n.a.	n.a.
CdT	26	0.02	755	154	19	0.011	-21	-40	n.a.	n.a.	n.a.	n.a.	n.a.	n.a.
CEL	1.5	0.01	741	305	18	0.010	-21	n.d.	0.60	0.001	-	0.62	299.8	0.0002
CIM-D	1.9	0.01	785	133	20	0.012	-18	n.d.	n.a.	n.a.	n.a.	n.a.	n.a.	n.a.
COR	1.1	0.01	815	341	20	0.010	-19	n.d.	n.a.	n.a.	n.a.	n.a.	n.a.	n.a.
FAL	2.1	0.01	821	115	21	0.012	-21	n.d.	0.92	0.004	-	0.44	295.5	0.0002
FAL2	15	0.02	815	344	20	0.011	-21	-41	n.a.	n.a.	n.a.	n.a.	n.a.	n.a.
FdC	1.1	0.01	813	340	20	0.012	-19.5	n.d.	0.47	0.001	0.23	1.01	294.4	0.0002
FdA	1.5	0.01	745	168	19	0.011	n.a.	n.a.	1.02	0.009	-	0.66	296.5	0.0001
ASC	11	0.04	795	333	20	0.011	-21	-20	n.a.	n.a.	n.a.	n.a.	n.a.	n.a.
FdSA	2.1	0.01	788	285	19	0.011	-22	n.d.	0.96	0.004	-	0.37	296.9	0.0002
MDT	2.1	0.01	785	285	20	0.012	-18.5	n.d.	0.95	0.004	-	0.79	297.5	0.0002
MdV	2.4	0.01	770	144	19	0.011	-18	n.d.	n.a.	n.a.	n.a.	n.a.	n.a.	n.a.
PAL	63	88	722	25	18	0.012	-30	-60	n.a.	n.a.	n.a.	n.a.	n.a.	n.a.
PAN	13	0.01	511	26	12	0.009	-18.1	n.d.	0.29	0.001	0.15	1.99	295.5	0.0003
PAN-S	59	615	313	0.21	8	0.007	-20.6	-62	0.54	0.002	0.38	1.22	296.8	0.0002
PIA	3.6	0.01	811	95	19	0.010	-20.5	n.d.	n.a.	n.a.	n.a.	n.a.	n.a.	n.a.
PI-C	6.1	0.05	620	89	15	0.010	-21.5	-53	0.89	0.004	-	0.52	295.4	0.0002
PI-P	71	57	615	11	15	0.009	-14	-85	0.59	0.002	-	0.76	296.5	0.0002
PIE-D	1.5	0.01	786	231	19	0.011	-22	n.d.	n.a.	n.a.	n.a.	n.a.	n.a.	n.a.
PaO	2.1	0.15	745	185	19	0.010	-21	-74	0.62	0.001	-	0.62	294.3	0.0004
R-FM	1.3	0.01	815	317	20	0.011	-21	n.d.	n.a.	n.a.	n.a.	n.a.	n.a.	n.a.
SAG	13	0.40	566	85	14	0.008	-8.5	-62	0.79	0.001	-	0.45	296.8	0.0001
S-GA	11	0.03	675	107	17	0.010	-20.5	-30	1.03	0.007	-	0.54	299.4	0.0001
S-LU	1.8	0.02	755	295	19	0.010	-22	-7.5	n.a.	n.a.	n.a.	n.a.	n.a.	n.a.
SVE	1.1	n.d.	812	326	20	0.012	n.a.	n.a.	n.a.	n.a.	n.a.	n.a.	n.a.	n.a.
TAR	16	3.1	658	21	16	0.010	-19.5	-85	1.04	0.006	-	0.68	297.7	0.0002
TOP	1.6	0.01	775	188	19	0.011	-21.5	n.d.	0.39	0.001	0.21	1.34	296.4	0.0001
TR-2	22	0.02	744	216	19	0.011	-21.5	-21	n.a.	n.a.	n.a.	n.a.	n.a.	n.a.
VIL	15	0.01	745	111	18	0.009	-20	n.d.	n.a.	n.a.	n.a.	n.a.	n.a.	n.a.
VFm	n.a.	n.a.	n.a.	n.a.	n.a.	n.a.	-20.9	-51	n.a.	n.a.	n.a.	n.a.	n.a.	n.a.
VFv	n.a.	n.a.	n.a.	n.a.	n.a.	n.a.	-18.9	-49	n.a.	n.a.	n.a.	n.a.	n.a.	n.a.

Figures

Figure 1: Geo-structural map of the MIB (Conti et al., 2020). The activity status of the main fault systems (Delle Donne, 2005) and location of the epicenters of historic and recent earthquakes (Saccorotti et al., 2022) are also reported.

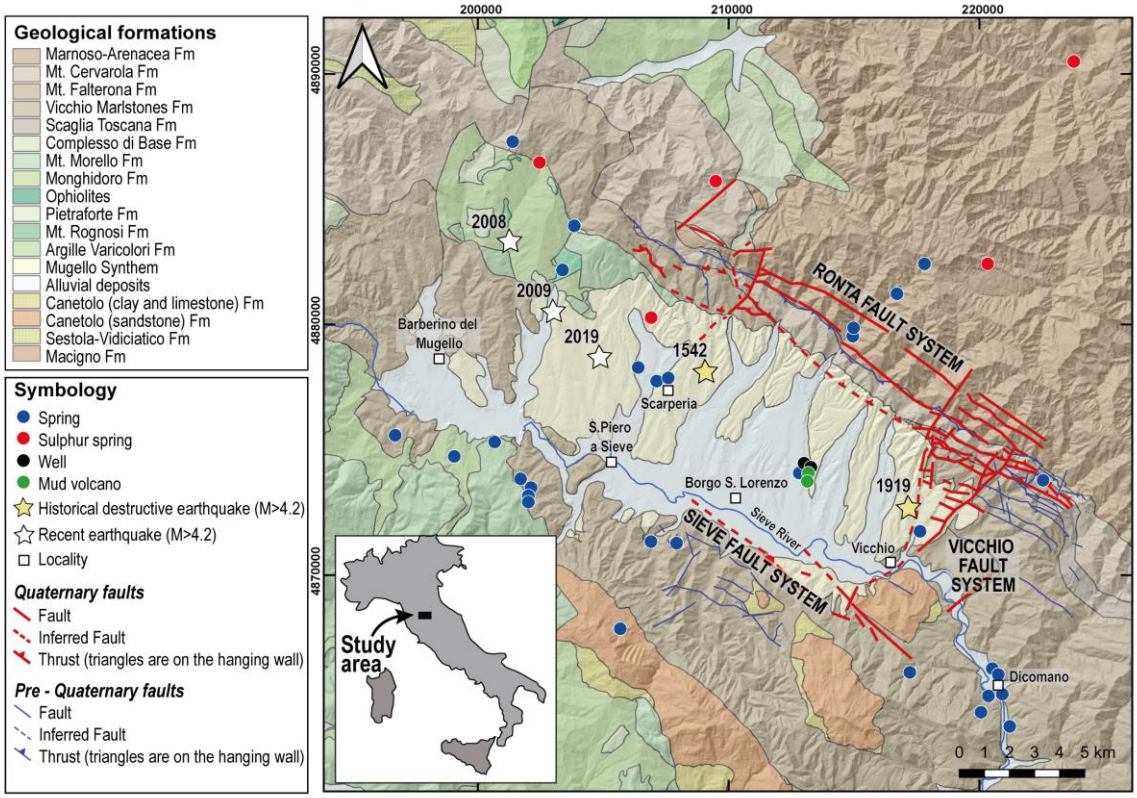

Figure 2: Water emergencies from selected sampling sites: (A) Casaglia (sulfur spring); (B) Panna Sulfurea (sulfur spring); (C) Sagginale (sulfur spring); (D) Fonte dell'Ascensione (cold spring); (E) Piandrati (cold spring) and (F) Bricciana (cold spring).

Figure 3: The Langelier-Ludwig diagram for the investigated samples: the different types of samples are reported in the legend (Tab. 1). SW indicates the average composition of seawater (data from Gibbs, 1970). IDs as in Table 1.

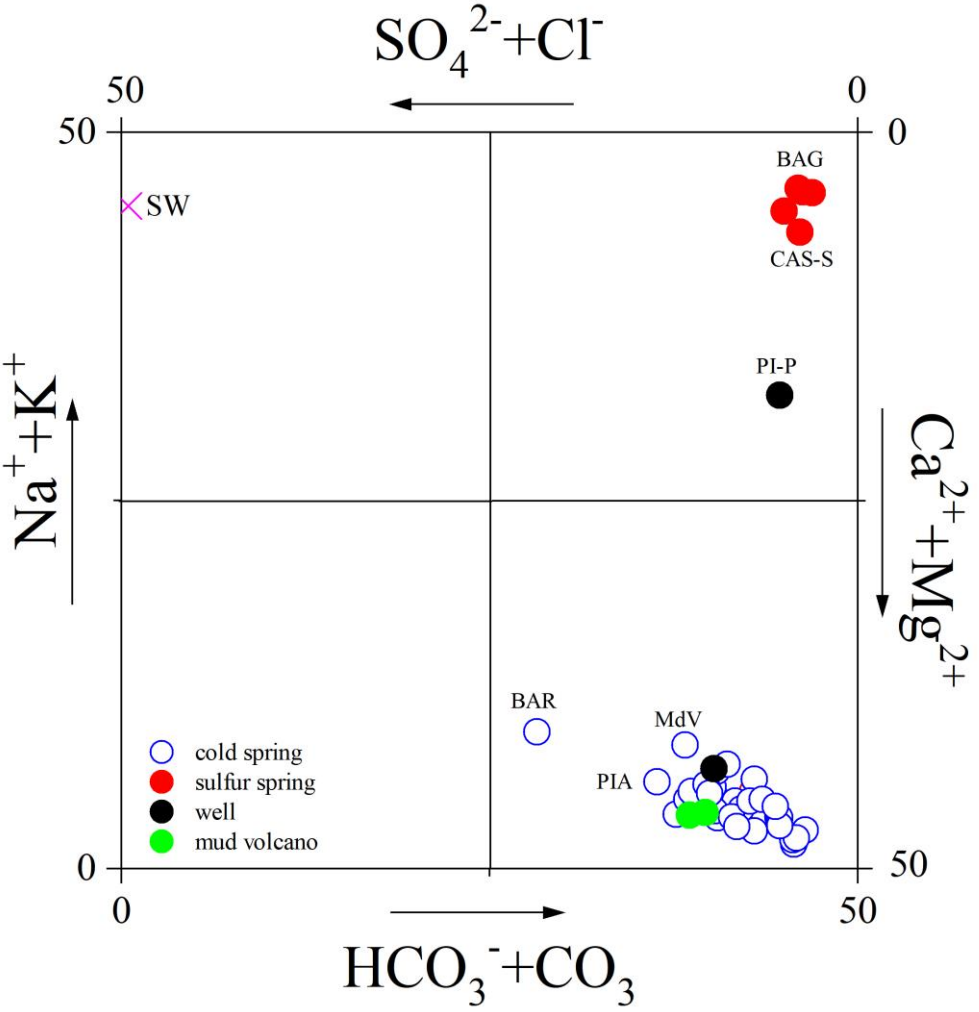

Figure 4: R/R_a vs. $^4He/^{20}Ne$ binary diagram. Mixing lines towards $R_c/R_a = 0.20$ and $R_c/R_a = 0.02$ are also reported. IDs as in Table 1.

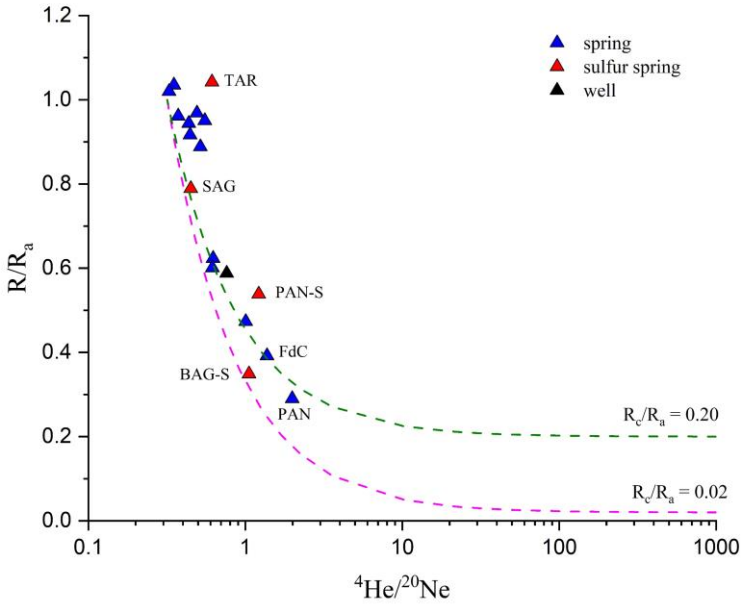

Figure 5: (a) δ^2H vs. $\delta^{18}O$ binary diagram, both expressed in ‰ (vs. V-SMOW), where the Global Meteoric Water Line (GMWL; Craig, 1961), the Central Italy Meteoric Water Line (CIMWL; Longinelli and Selmo, 2003) and the Mediterranean Meteoric Water Line (MMWL; Gat and Carmi, 1970) are also reported. (b) $\delta^{18}O$ vs. altitude (in m a.s.l) binary diagram, where the two gradient G_1 (from Longinelli and Selmo, 2003), G_2 (from Vaselli and Minissale, 2011) and G_3 (from Giustini et al., 2016) are also drawn. (c) δ^2H v. altitude (in m a.s.l) binary diagram, where the apparent gradient computed for the investigated samples is also reported.

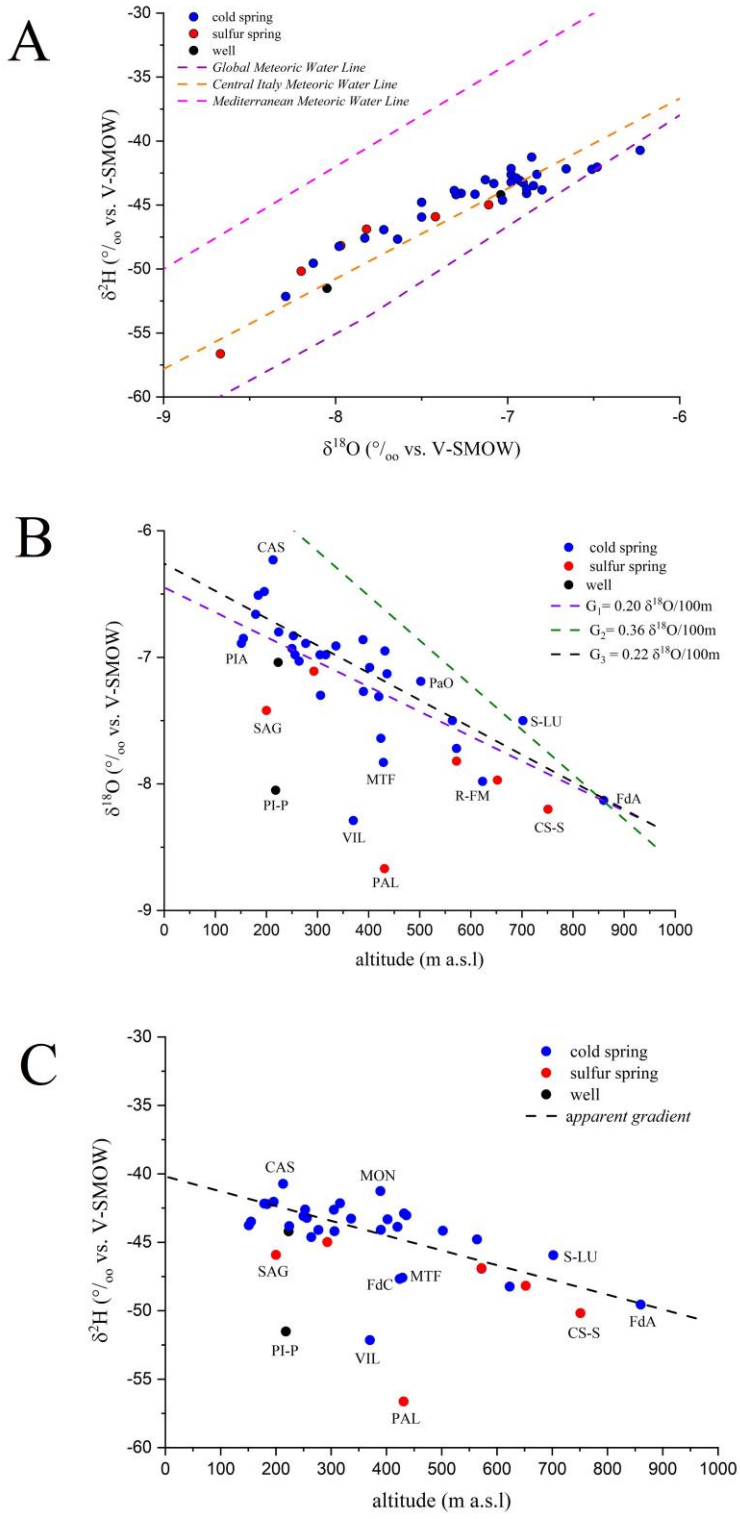

Figure 6: (a) (Ca^{2+}+Mg^{2+}) vs. (HCO_3^-+CO_3^{2-}) binary diagram; (b) (Ca^{2+}+Mg^{2+}) vs. SO_4^{2-} binary diagram. Values are in meq/L. IDs as in Table 1.

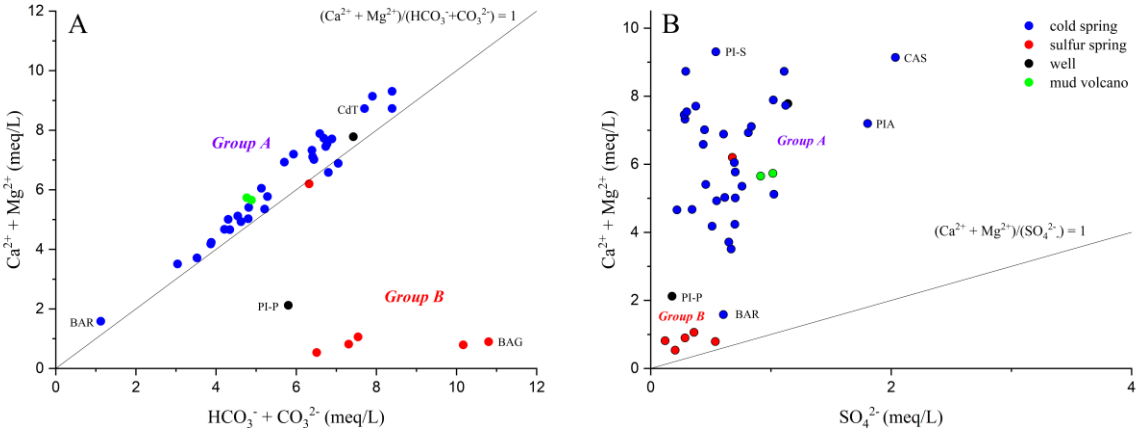

Figure 7: Na^+ vs. Cl^- (in meq/L) binary diagram. IDs as in Table 1. The stochiometric line referred to halite dissolution as well as the tendency of the Group B waters to be characterized by Na-excess are also reported.

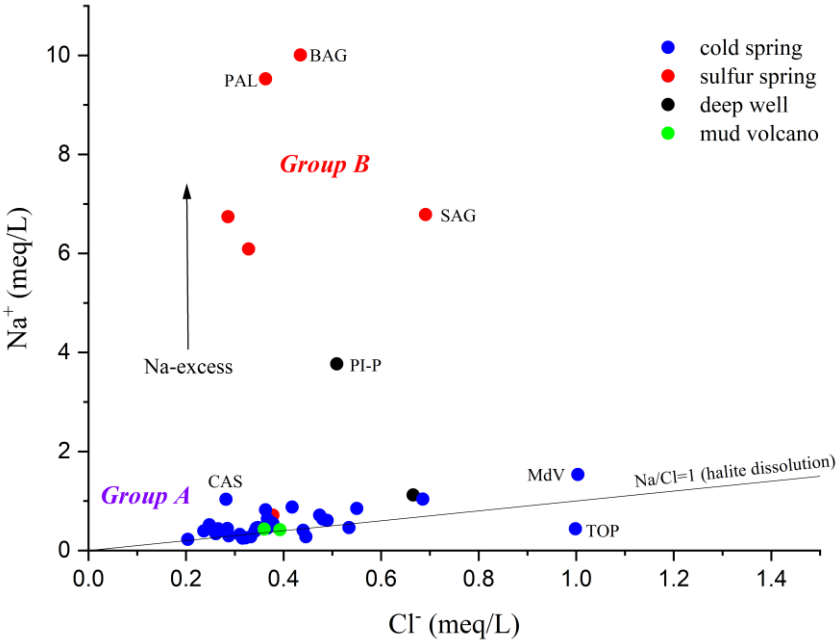

Figure 8: (10^3*B)/Cl vs. Na (in mg/L) binary diagram. The diagram shows the considerable increase in boron detected for the *Group B* waters with respect to Cl, as a consequence of long-lasting interactions with silicates.

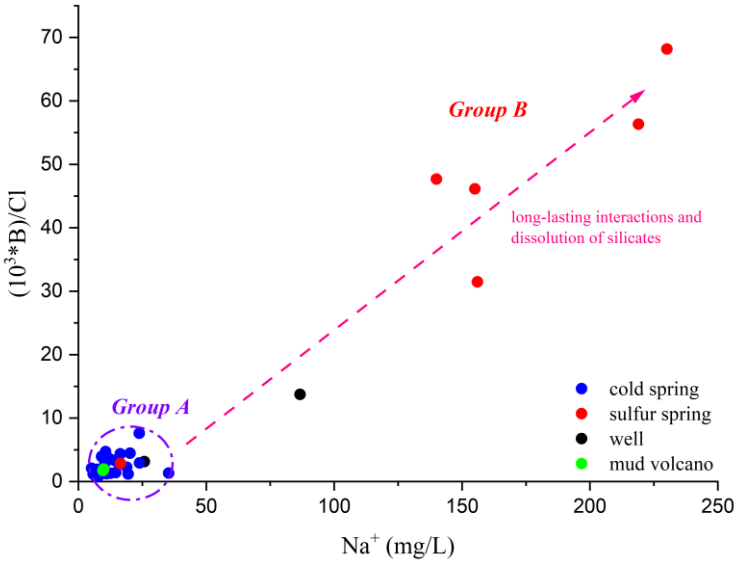

Figure 9: log[(aNa^+)/(aH^+)] vs. log(aH_4SiO_4) activity diagrams. The stability fields for albite, gibbsite and kaolinite are also reported. The dashed circle indicates the Group B waters (modified from Bowers et al., 1984). The saturation Index (SI) was calculated through PHREEQC software (Parkhust and Appelo, 1999), using the concentrations of dissolved ions, pH and Eh as input data.

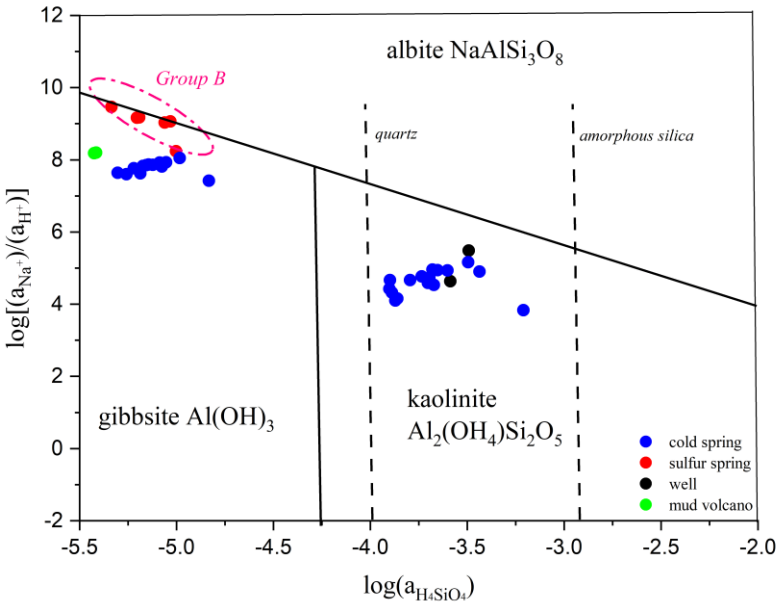

Figure 10: Ar-N_2-O_2 ternary diagram for the dissolved gases samples. The mixing line between atmospheric gases and an O2-depleted reducing gas phase is reported.

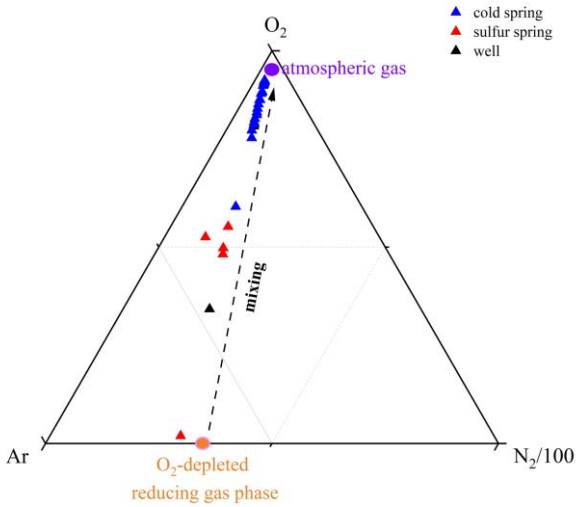

Figure 11: δ^{13}C-CO_2 vs. δ^{13}C-CH_4 (both expressed in ‰ vs. V-PDB) binary diagram. The boxes report the average carbon isotopic ratios for different genetic processes: organic (biogenic), thermogenesis and dissolution of atmospheric gases. Reference values for δ^{13}C-CO_2 and δ^{13}C-CH_4 are from Whiticar (1999) and Merritt et al. (1995). IDs as in Table 1.

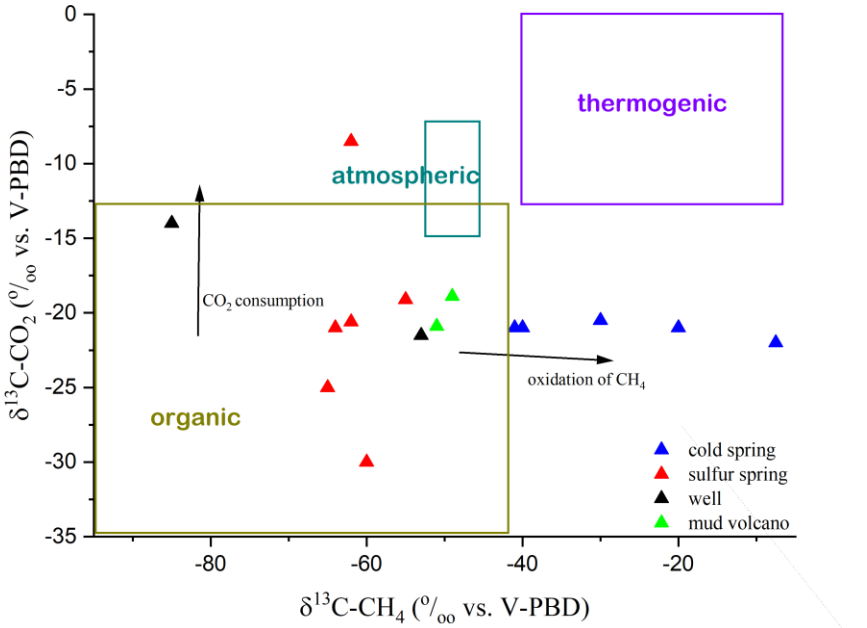

Figure 1

Click here to access/download;Figure;Fig. 1.jpg

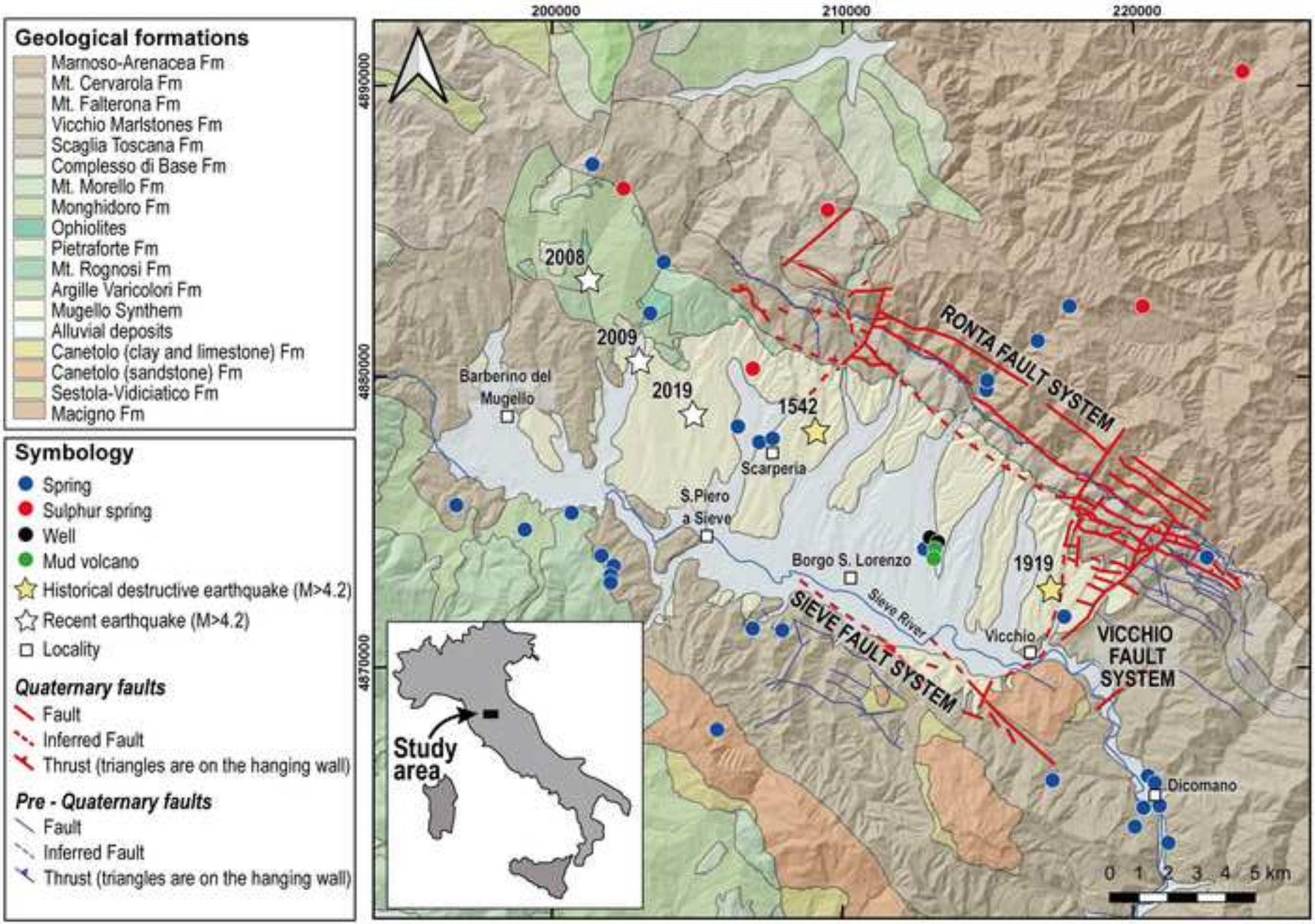

Figure 2

Click here to access/download;Figure;Fig. 2.jpg

Figure 3

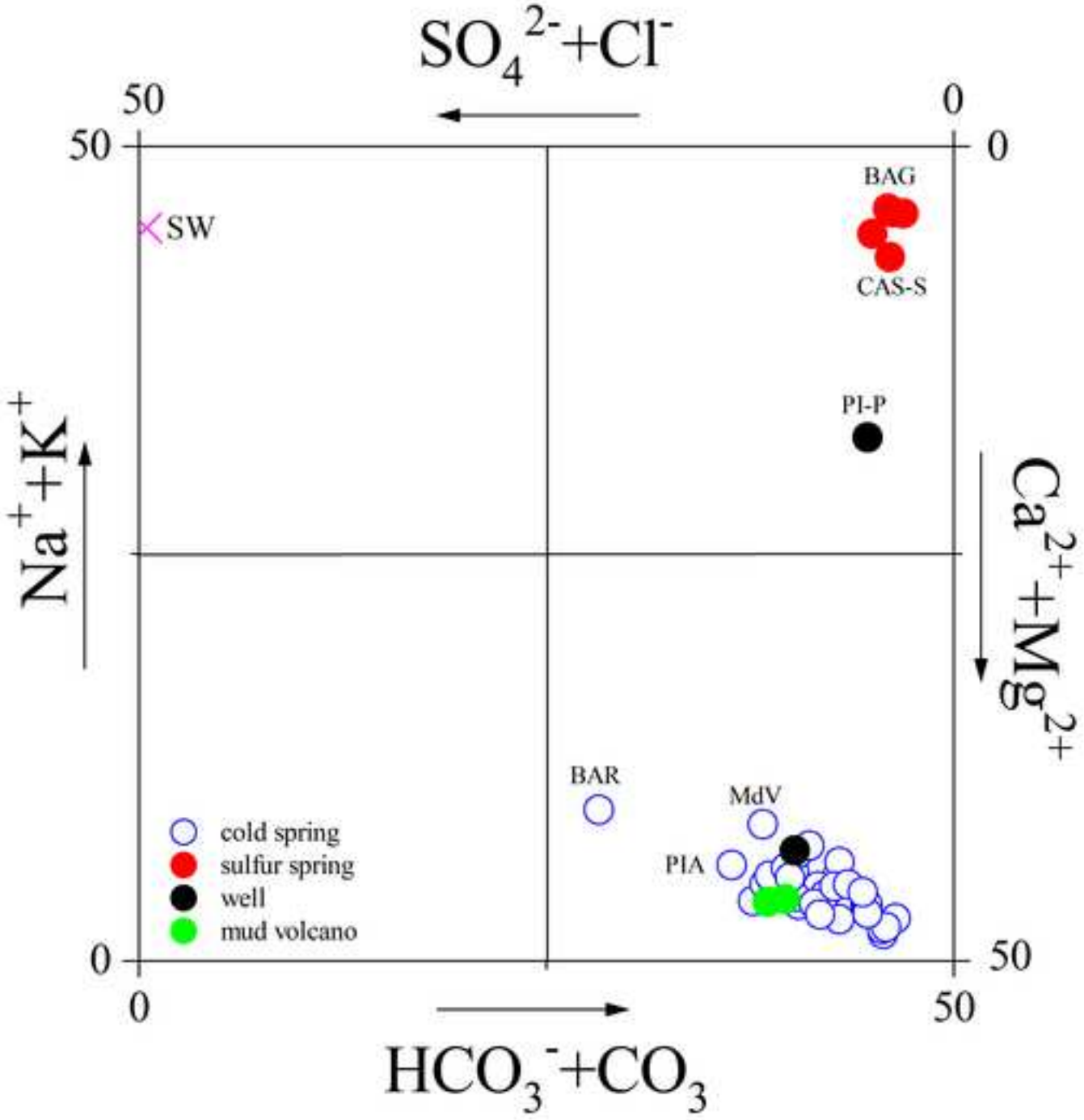

Figure 4

Click here to access/download;Figure;Fig. 4.jpg

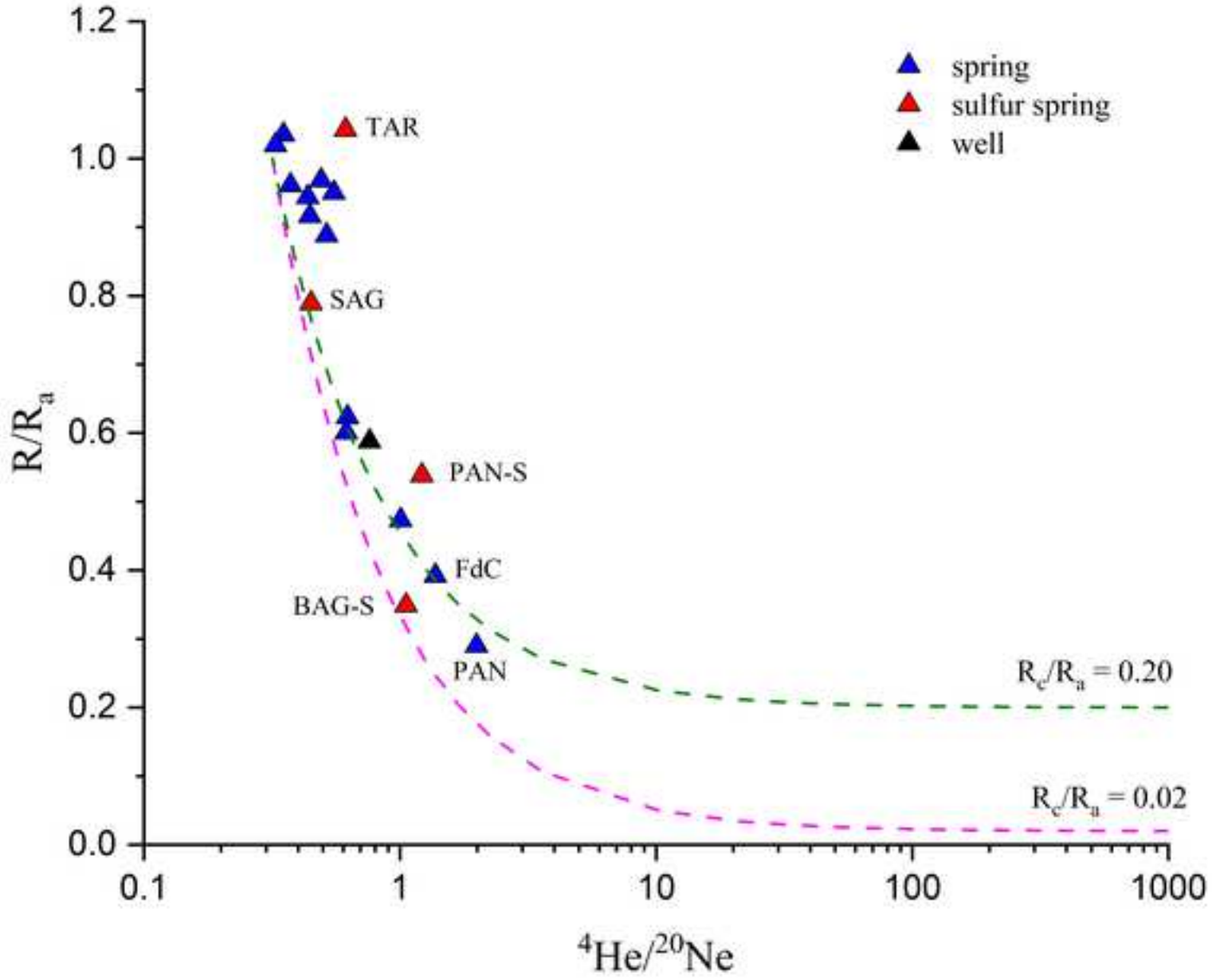

Figure 5

Click here to access/download;Figure;Fig. 5.jpg

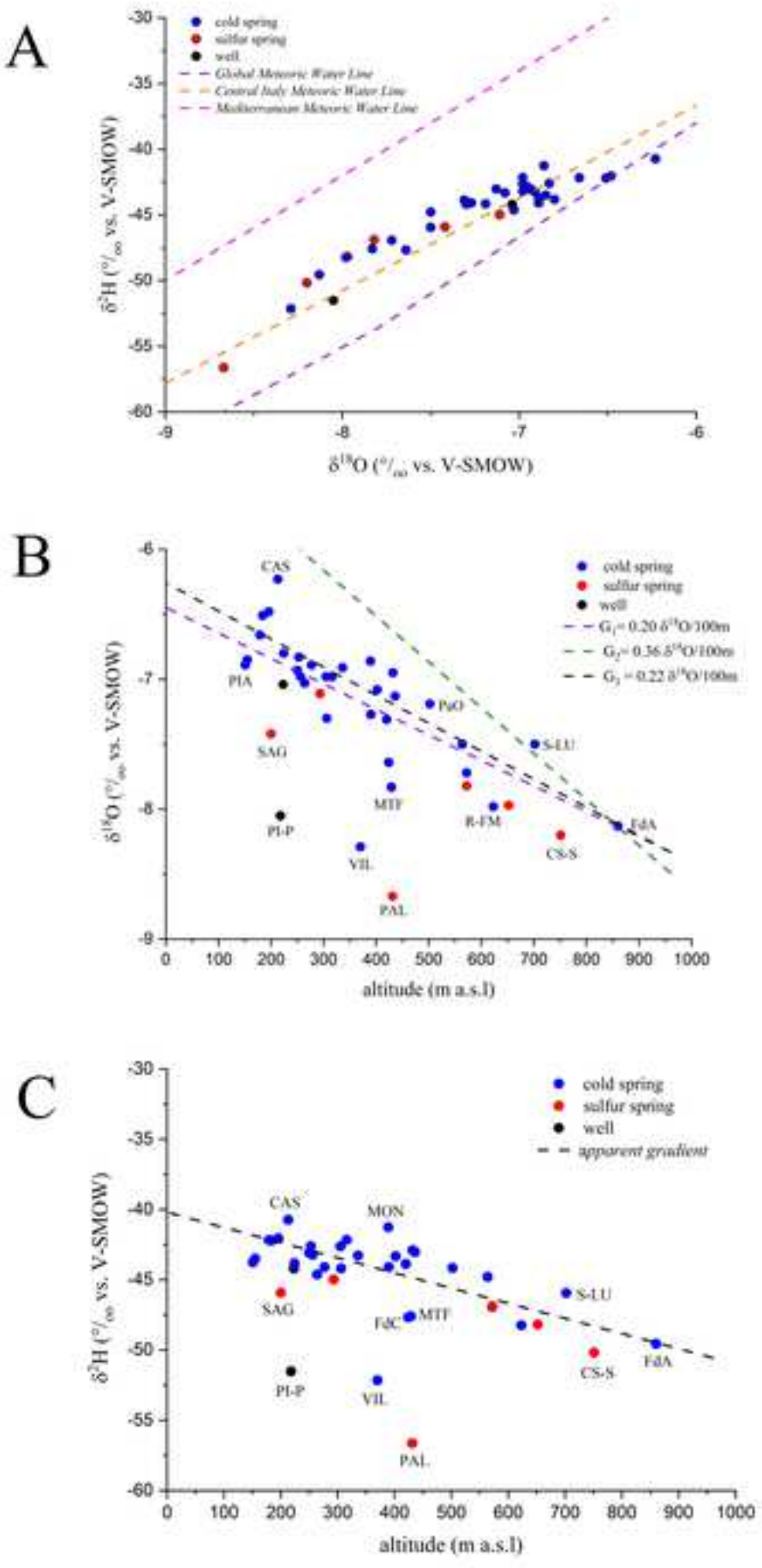

Figure 6

Click here to access/download;Figure;Fig. 6.jpg

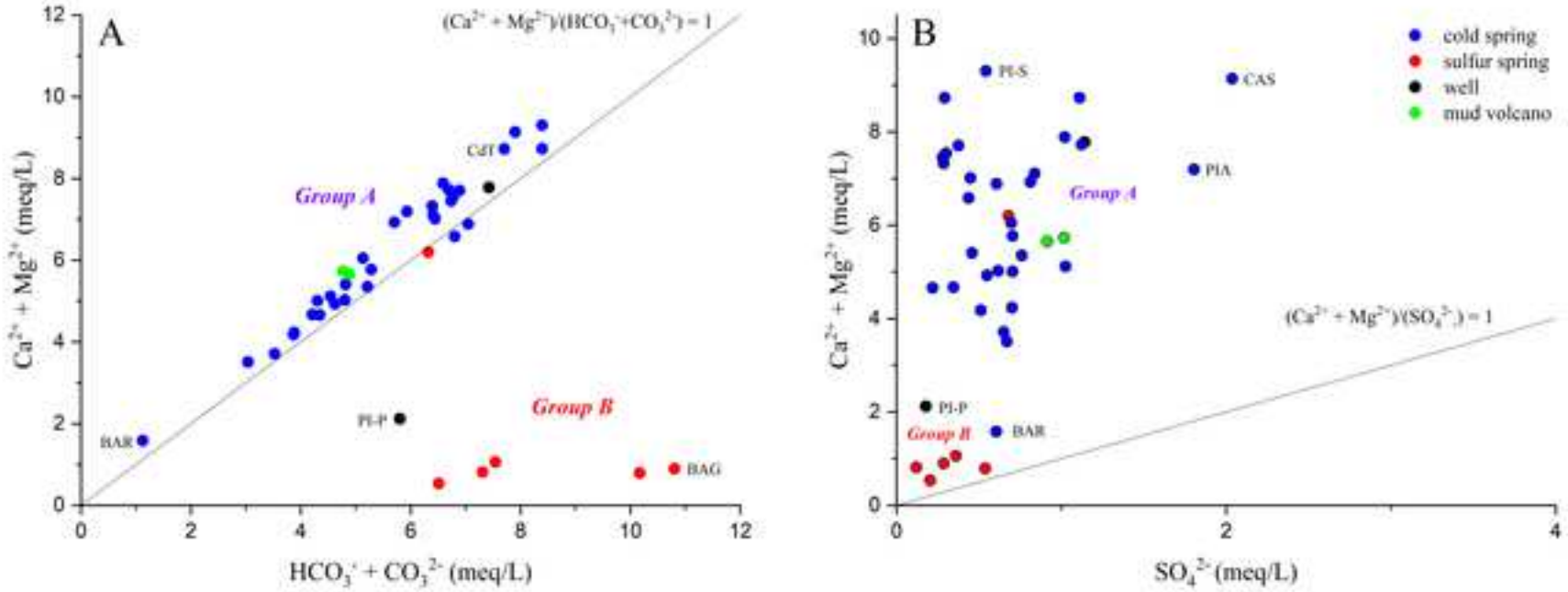

Figure 7

Click here to access/download;Figure;Fig. 7.jpg

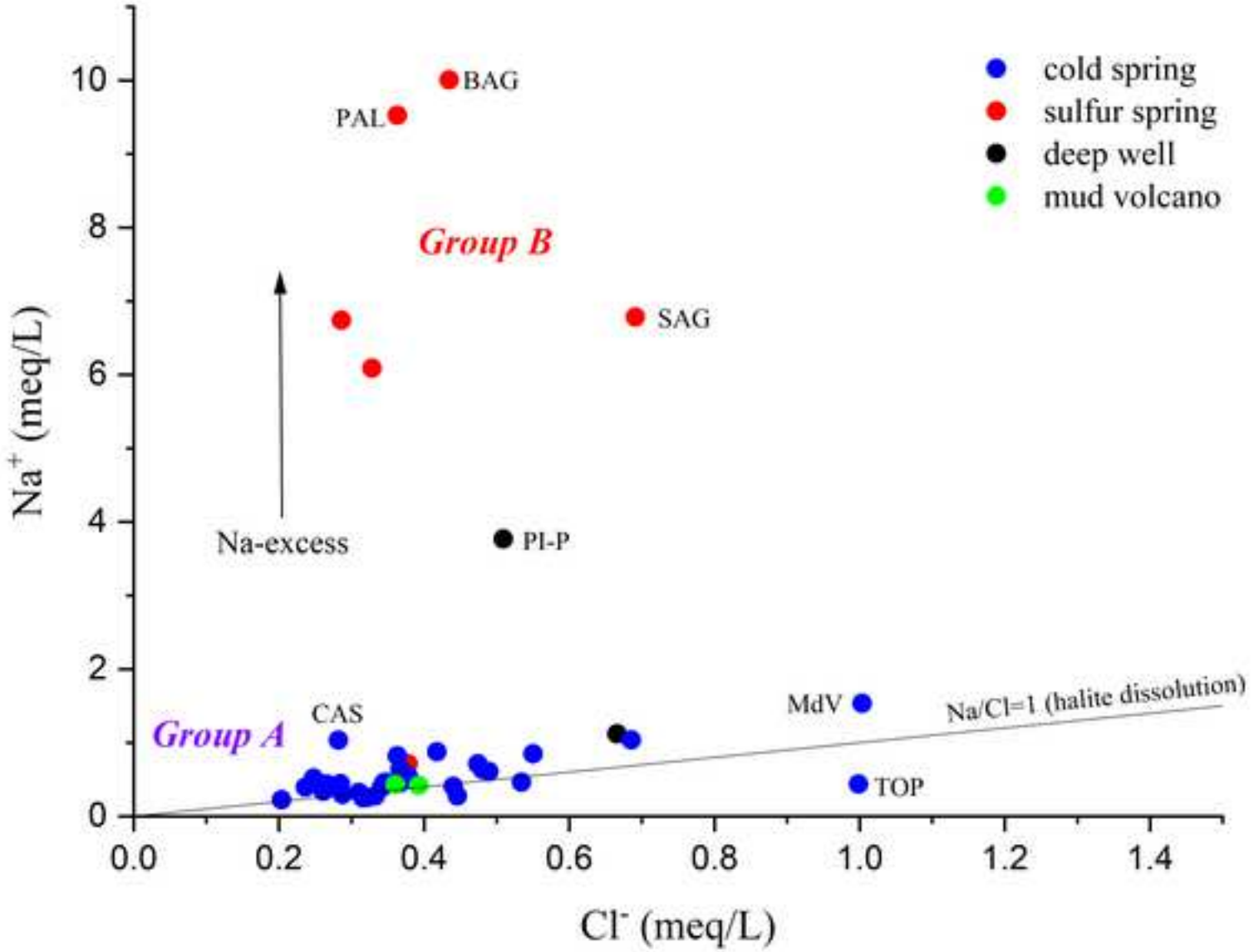

Figure 8

Click here to access/download;Figure;Fig. 8.jpg

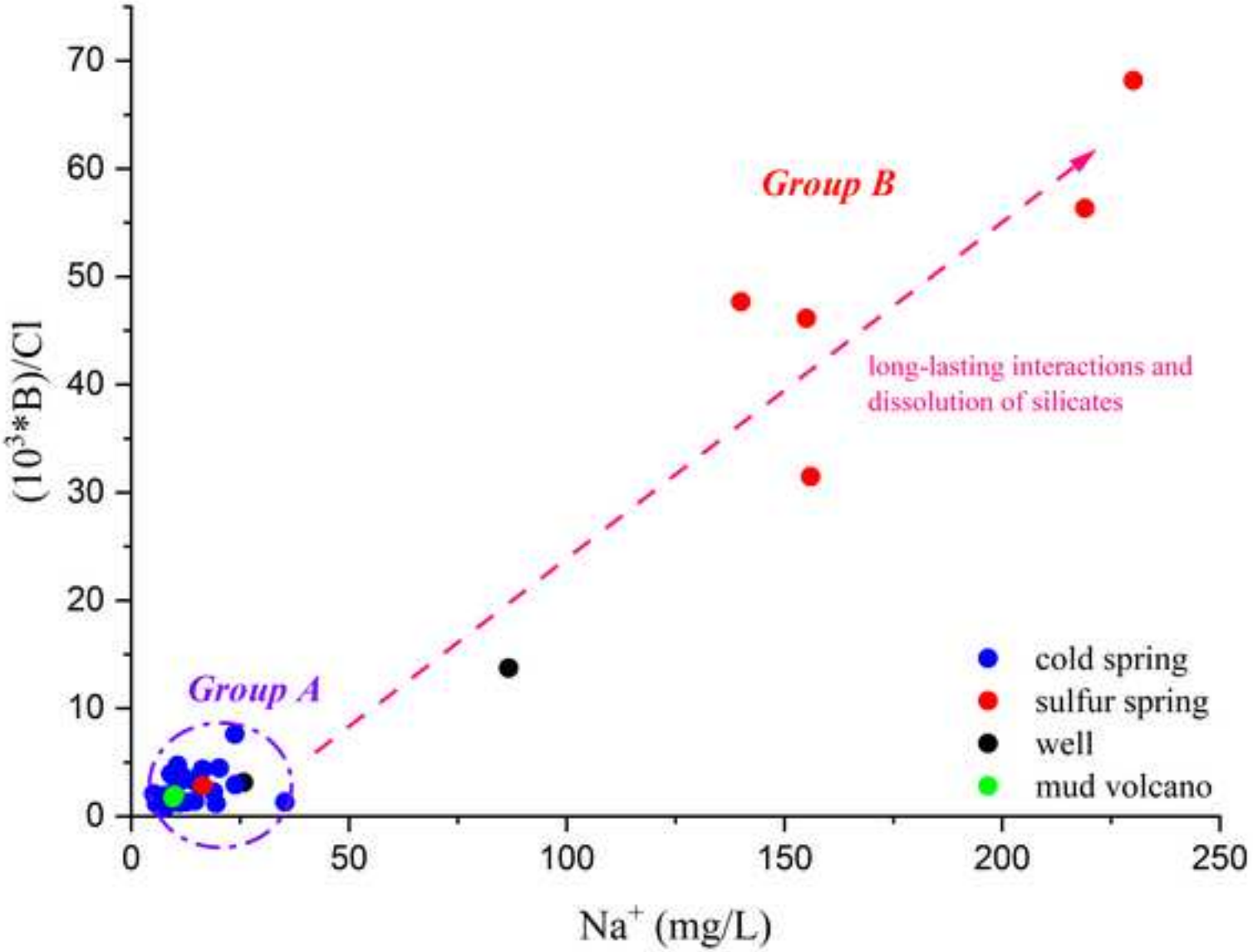

Figure 9

Click here to access/download;Figure;Fig. 9.jpg

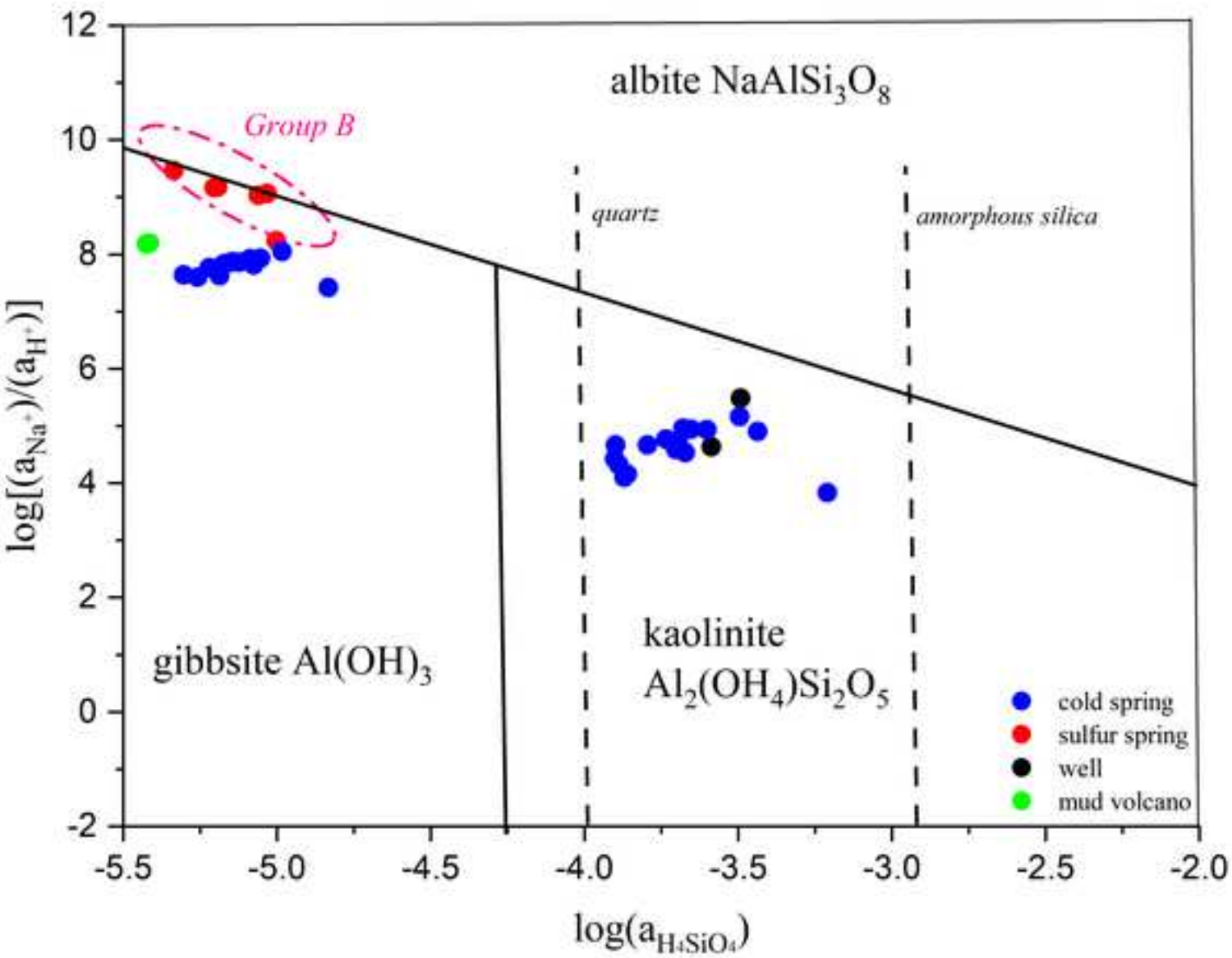

Figure 10

Click here to access/download;Figure;Fig. 10.jpg

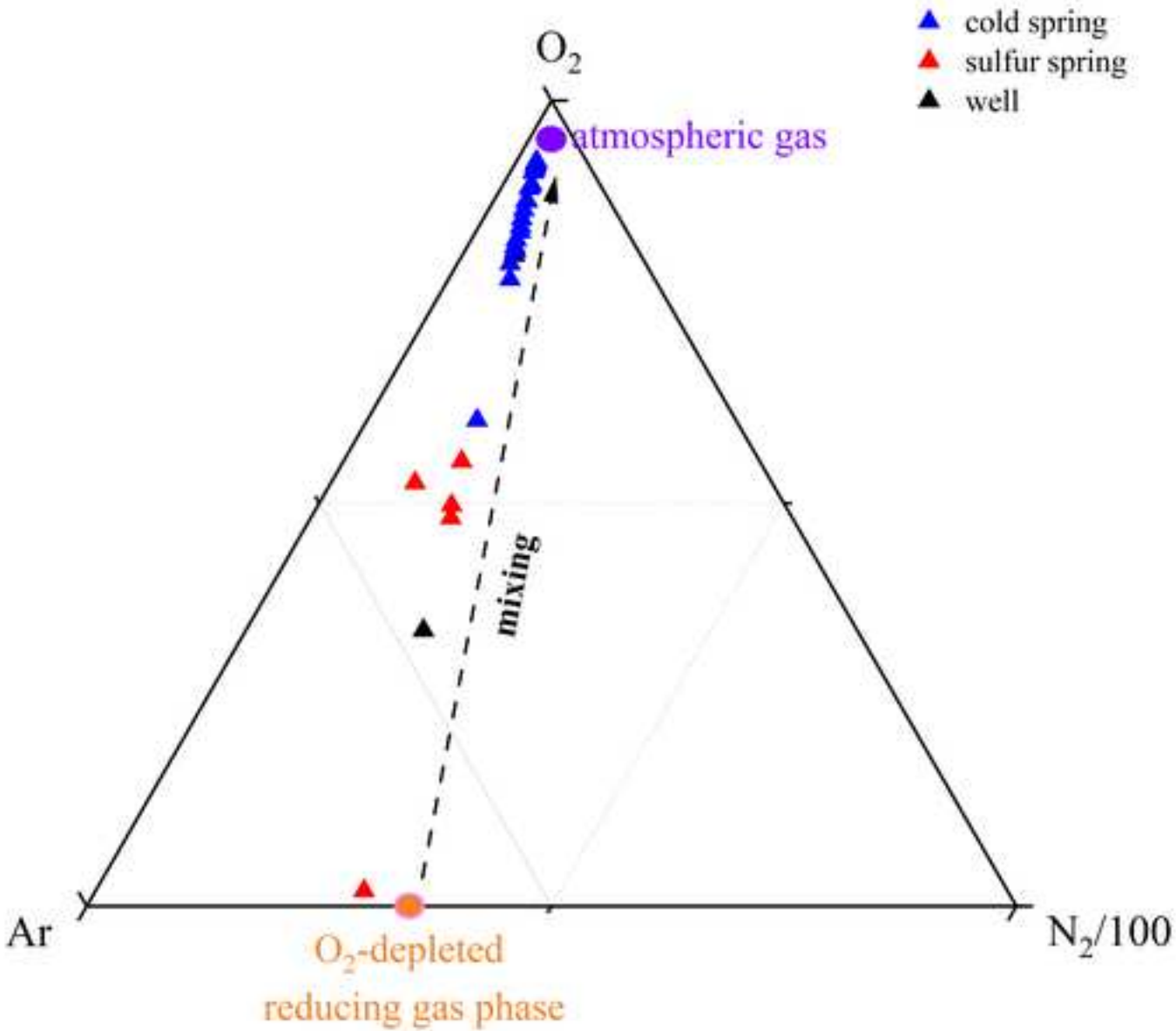

Figure 11

Click here to access/download;Figure;Fig. 11.jpg